INVESTIGATION OF OZONE TREATMENT ON MECHANICAL PROPERTIES OF ORIENTED CARBON NANOTUBE/EPOXY NANOCOMPOSITES

by

ZEKİ SEMİH PEHLİVAN

Submitted to the Graduate School of Engineering and Natural Sciences

in partial fulfillment of

the requirements for the degree of

Master of Science.

Sabanci University

Fall 2016

APPROVED BY:

Asst. Prof. Dr. Fevzi Çakmak Cebeci
(Thesis Supervisor) .....

Assoc. Prof. Dr.Burç Mısırlıoğlu .....

Asst. Prof. Dr. Elif Özden Yenigün .....

DATE OF APPROVAL: 06.01.2017

ABSTRACT

INVESTIGATION OF OZONE TREATMENT ON MECHANICAL PROPERTIES OF ORIENTED CARBON NANOTUBE/EPOXY NANOCOMPOSITES

Zeki Semih Pehlivan

Mechatronics Engineering, MSc. Thesis, 2016

Thesis Supervisior: Asst. Prof. Fevzi C.Cebeci

Keywords: Vertically Aligned Carbon Nanotubes, Polymer Nanocomposites, Ozone treatment, Dynamical Mechanical Analysis

With the discovery of spectacular mechanical properties of carbon nanotubes (CNTs), CNTs became one of the most important reinforcement materials for composite materials. Many polymer-CNT combinations have been studied for various applications. Although, composition of an epoxy as matrix material and vertically aligned carbon nanotubes (VA-CNTs) as reinforcement is the best candidate for structural components.

In this study, VA-CNTs for nanocomposite applications have been synthesized by catalytic chemical vapor deposition (CCVD) technique, and parameters such as catalyst structure and process recipe have been optimized to improve quality of VA-CNTs for further steps. To determine the quality of VA-CNTs, graphitization level, oxidation temperature, purity and morphology of CNTs have been measured. For purity and oxidation temperature tests, thermogravimetric analysis (TGA); for graphitization level measurements, RAMAN spectroscopy; for morphological analysis, scanning electron microscopy (SEM) have been employed.

After synthesis and characterization steps, VA-CNTs have been treated with ozone to increase interaction between epoxy and CNTs. This interaction has been measured with contact angle measurements. Then, epoxy/CNT nanocomposites have been produced and mechanical performances have been tested to compare direct effect of ozone treatment on the mechanical properties of nanocomposites. For mechanical tests, tension mode of dynamical mechanical analysis (DMA) has been used.

ÖZET

OZONLAMA İŞLEMİNİN YÖNLENDİRİLMİŞ KARBON NANOTÜP/EPOKSİ NANOKOMPOZİTLERİNİN MEKANİK ÖZELLİKLERİNE ETKİLERİNİN İNCELENMESİ

Zeki Semih Pehlivan

Mekatronik Mühendisliği, Yüksek Lisans Tezi, 2016

Tez Danışmanı: Yrd. Doç. Fevzi Ç. Cebeci

Anahtar Kelimeler: Dikey Yönelimli Karbon Nanotüp, Polimer Nanokompozite, Ozonlama İşlemi, Dinamik Mekanik Analiz

Mükemmel mekanik özelliklerinin keşfedilmesi sonucu karbon nanotüpler (KNT) kompozit malzemeler için en önemli takviye malzemesi haline geldiler. Farklı uygulamalar için birçok farklı polimer-KNT kombinasyonu denendi; ancak yük taşınımının önem kazandığı uygulamalar için matris malzemesi olarak epoksi, takviye malzemesi olarak yönelimli karbon nanotüplerin (Y-KNT) kullanıldığı nanokompozitler en başarılı kombinasyonu oluşturmaktadır.

Bu çalışmada, nanokompozit uygulamaları için yönelimli karbon nanotüpler katalitik kimyasal buhar biriktirme tekniği ile üretildi ve katalizör yapısı, proses reçetesi gibi parametreler karbon nanotüpün ileriki adımlar için kalitesini arttıracak şekilde optimize edildi. Üretilen yönlendirilmiş karbon nanotüplerin kalitesi, karbon nanotüplerin saflığı, oksitlenme sıcaklığı, grafitleşme seviyesi ve morfolojisi test edilerek ölçüldü. Saflık ve oksitlenme sıcaklığının belirlenmesinde termogravimetrik analiz (TGA), grafitleşme seviyesinin belirlenmesinde RAMAN spektroskopisi, morfoloji çalışmalarında ise taramalı electron mikroskobu (SEM) kullanıldı.

Üretim ve karakterizasyon aşamaları sonrasında yönelimli karbon nanotüpler ozonlama işlemine maruz bırakılarak, karbon nanotüpler ile epoksi arasındaki etkileşim arttırılmaya çalışıldı. Bu etkileşim kontak açı ölçümleri ile gözlemlendi. Bu işlemden sonra epoksi/KNT kompozitleri üretilerek ozonlama işleminin mekanik özellikler üzerindeki etkisinin doğrudan gözlemlenebilmesi için numunelere dinamik mekanik analiz testleri yapıldı.

ACKNOWLEDGEMENTS

First of all, I would like to thank my thesis advisor Asst. Prof. Fevzi Ç. Cebeci for accepting me as a master student and giving me the opportunity to complete my study. I could not be able to finish my thesis without his support, guidance and encouraging advises.

I also would like to thank Asst. Prof. Hulya Cebeci (ITU) for sharing laboratory facilities for almost three months and felt me as her student.

I am very thankful to Deniz Kavrar Urk. She gave me a precious head start with her great experience at the beginning of this study and kept me on track whenever I got lost. I could not complete this work on time without her helps and support. I am indebt her.

I am grateful to my group mates, Esin Ates Güvel, Yonca Belce, Deniz Koken, Buket Alkan, Melike Barak and Araz Sheibani Aghdam for positive and creative environment that they created.

I also need to take every single member of ITU-Aerospace Research Center for welcoming environment and their hospitality. They made me feel like a member of group and there was always someone to help me out whenever I had problem. I really appreciate it.

I also thank SUNUM staff who helped me while learning setups that I use in my experiments. I am really thankful to their experience shared with me. I am also thankful to Didem Ovali and Abdullah Dönmez from Istanbul Technical University for their help on my analysis.

Most importantly, I want to thank my family who always trusted and stood behind me. None of this can be possible without them.

TABLE OF CONTENTS

LIST OF FIGURES

LIST OF TABLES

LIST OF SYMBOLS AND ABBREVATIONS

A-CNT	Aligned Carbon Nanotube
AFM	Atomic Force Microscopy
Al_2O_3	Alumina
C_2H_4	Ethylene
CCVD	Catalytic Chemical Vapor Deposition
CVD	Chemical Vapor Deposition
CNT	Carbon Nanotube
DMA	Dynamical Mechanical Analyses
MWCNT	Multi-Walled Carbon Nanotube
PE-CVD	Plasma-Enhanced Chemical Vapor Deposition
PNC	Polymer Nanocomposite
SEM	Scanning Electron Microscopy
SiO_2	Silica
SWCNT	Single-Walled Carbon Nanotube
T_g	Glass Transition Temperature
TGA	Thermogravimetric Analysis
VA-CNT	Vertically Aligned Carbon Nanotube
VASE	Various Angle Spectroscopic Ellipsometer
VLS	Vapor-Liquid-Solid

CHAPTER 1 Introduction

1.1 Brief Introduction to Carbon Nanotubes

In the early 1990s, after a few years of development of fullerene, closed cage-like structure of carbon atoms that made of hexagonal and pentagonal surfaces, long and slender form of fullerene [1], carbon nanotubes (CNTs) where walls of tube is hexagonal carbon were discovered [2]. Since their discovery, carbon nanotubes have been attracting the attention of scientists not only for their unique physical and chemical properties such as mechanical, thermal and electrical properties but also theirs wide range of possible applications [3].

Carbon nanotubes can be imagined as a rolled sheet of graphite. Since graphite is a layer of carbon atoms in hexagon structure, carbon nanotubes can get different atomic array due to different direction of rolling. Hence, all properties of nanotubes are depended on how graphite layer rolled; since, arrangement of carbon atoms is decided by that.

The atomic structure of nanotubes is described in of tube chirality which is defined by the chiral vector C_h, and the chiral angle, θ. The chiral vector represents the direction of rolling-up and described by the equation [4]:

$$C_h = na_1 + ma_2$$

where coefficient n and m are the number of steps along carbon bonds of the hexagonal structure and, a_1 and a_2 are the unit vectors shown in Figure 1.1 [5].

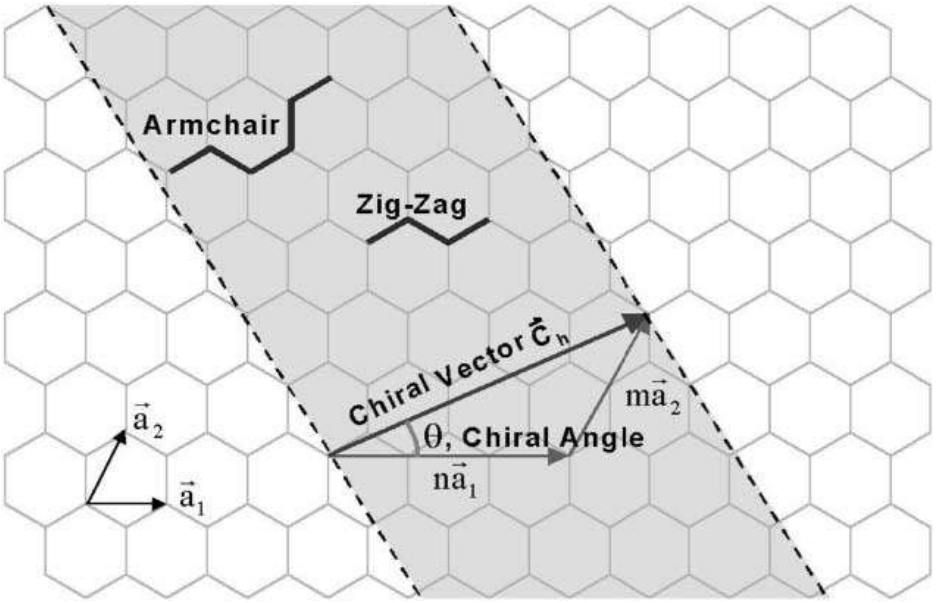

Figure 1.1. Schematic showing of how a graphite sheet is rolled to different types of carbon nanotubes

The angle of 0° and 30° are the critical chiral angles and are referred as zig-zag and armchair respectively based on geometry of carbon bonds. This structural difference mainly determines the electrical properties of CNTs [6]. Beside of that, geometry of carbon bonds has influence on elastic stiffness of CNTs [7]. Therefore, it can be concluded that chiral vector affects both electrical and mechanical properties of CNTs.

Carbon nanotubes can be classified in two groups by number of walls: single-walled carbon nanotubes (SWCNTs) and multi-walled carbon nanotubes (MWCNTs). MWCNTs are simply composed of concentric SWCNTs. There are four primarily used production methods for synthesize SWCNTs and MWCNTs. These methods are arc-discharge [8], laser ablation [9], gas-phase catalytic growth from carbon monoxide [10] and chemical vapor deposition (CVD) from hydrocarbons [11]. Chemical vapor deposition is the best candidate to produce CNTs for composite applications because of its potential of large scale production and tunability.

Carbon nanotubes are thought as perfect additive for load carrying in early 1990s with work of Overney et al. which was the calculation of Young's modules of short single walled carbon nanotube. The calculated young's modules was 1.5 TPa [12]. In addition to that, the first mechanical measurement which are made on MWCNTs gave young's module between 0.7 and 1.3 TPa by measuring intrinsic thermal vibrations of CNTs

with transmission electron microscope [13,14]. Moreover, the first directional measurement, where atomic force microscope (AFM) was employed, gave an average young's modules of 1.28 TPa [14]. Due to these exceptionally high mechanical properties of CNT, it is attracted lots of researchers' attention to use them as an additive material for polymer matrix nanocomposites.

1.2 Literature Review

1.2.1 Carbon Nanotube Synthesis

CNTs are firstly, synthesized with electric-arc discharge method by Iijiama et al. this technique generally contains two graphite rods as electrodes (shown in Figure 1.2). A voltage is applied on these rods under a helium atmosphere to achieve arc. Since anode rod consumes while process, distance between rods are kept stable by adjusting the position of anode. During decomposition of anode, nanotube containing soft fibrous material gathers on cathode side. To obtain SWCNTs, metallic catalyst particles are added to electrodes [5, 13–17].

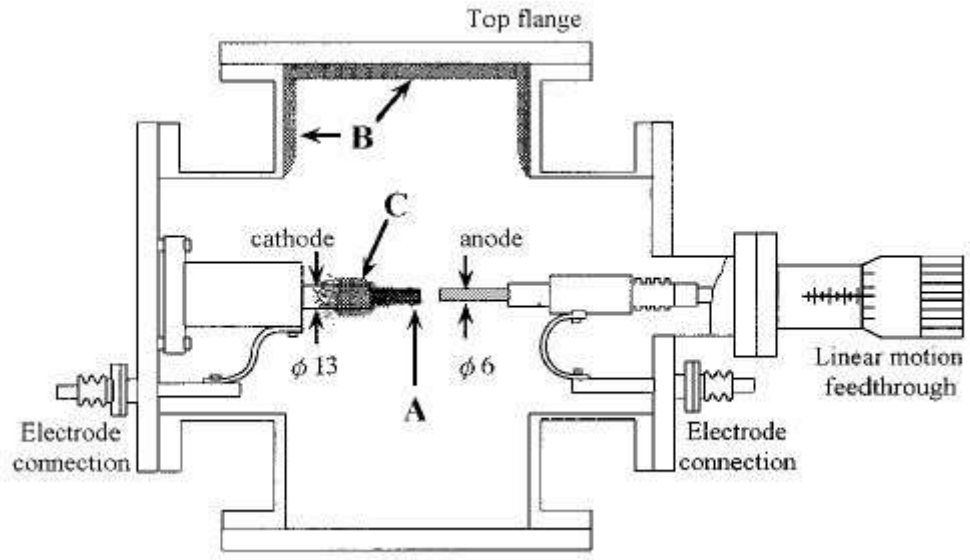

Figure 1.2. Schematic view of typical electric-arc discharge technique

Laser ablation method is another commonly used method to produce CNTs. In this method, a laser is employed to heat metallic particle containing graphite target. Target

is heated up to vaporize, then condensed material is collected as CNTs [7,19,20]. Typical setup of laser ablation technique is shown in Figure 1.3 [22]

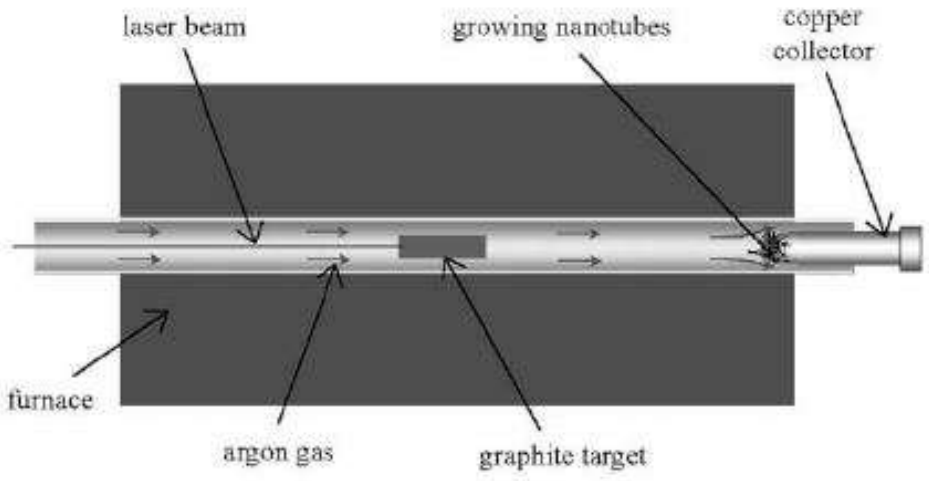

Figure 1.3. Schematic view of laser ablation setup

Beside of any advantages of both electric-arc discharge and laser ablation technique, these methods are limited by producing high volume of sample; moreover, purification step is needed to remove undesired side-products and obtain CNTs. As a result of that, gas phase carbon source involved production methods are developed such as chemical vapor deposition (CVD) technique. In CVD technique, hydrocarbons such as methane (CH_4), ethylene (C_2H_4), acetylene (C_2H_2) etc. are used as carbon source [10]. One or combination of these carbon precursors are broken-down in an inert environment then CNTs form on catalyst material which can be placed on a substrate or as free-standing [22–24].

One of the most important advantages of CVD processes is purity of CNTs are very high compared to other methods which enables to remove purification step. In addition, relatively large scale productions are possible since carbon source in gas phase can be replaced continuously by gas flow. In addition, this method allows producing highly aligned CNTs (A-CNTs) most likely vertically [26]. Yield of processes are compared in Table 1.1 [27].

Table 1.1. Characteristic comparison of CNT growth methods

Method	Temperature (°C)	Growth Rate (µm/s)	CNT Length (µm)	Yield	Quality	Purity
Laser ablation	~1200	0.1	1	Low	High	Medium
Arc-discharge	>3000	Up to 10^7	1	Low	Low	Low
Thermal CVD	500-1200	0.1-10	10^5	High	Medium	High

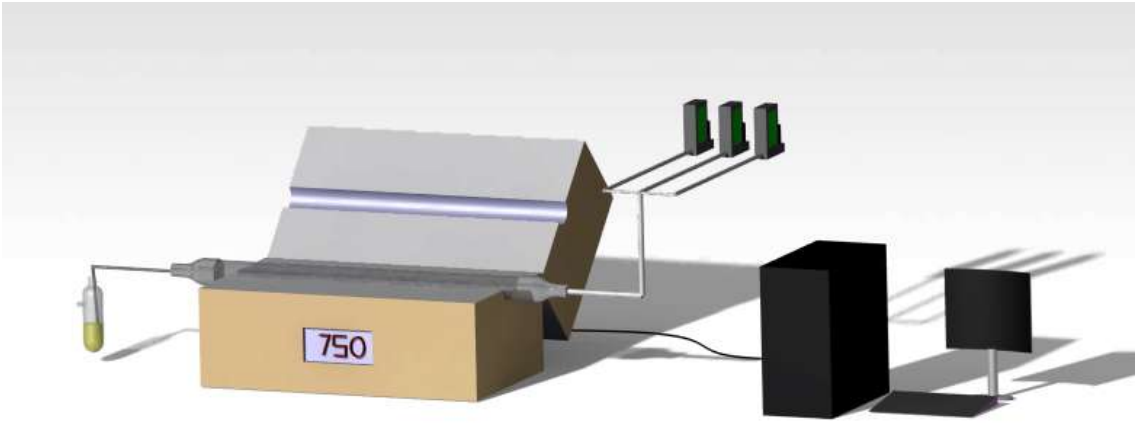

Figure 1.4. Schematic view of typical CVD setup

Many groups have reported different CVD process parameters to produce A-CNTs. One of the early studies was done by Rao et al. [28] In this work, pyrolysis of ferrocene around 900 °C was used to grow A-CNTs on silica substrate. In another work, Dai and co-workers have synthesized vertically positioned MWCNTs to substrate by pyrolysis of iron (II) phthalocyanine in Ar/H_2 atmosphere. Alignment of CNTs was perpendicular to substrate and have a uniform distribution of length and diameter [29].

In another study, Hart and his co-workers achieved millimeter long vertically aligned carbon nanotubes (VA-CNTs) on thin film of catalyst that is coated on a substrate by e-beam evaporation technique. Fe/Al_2O_3 was used as catalyst and process was done under H_2/Ar atmosphere. Most important outcomes of this work are achievement of rapid growth (millimeter long CNTs in 15 minutes) and importance of nucleation step, which makes catalyst chemically active before growth step starts, on CNT morphology [30].

All of these studies and many others are motivated researchers to investigate the growth mechanism of CNTs in CVD process. Due to that, it is been discovered that growth mechanism of CNT on CVD starts with super-saturation of catalyst, and two main growth models depend on position of catalyst particle, tip growth and root growth, were developed. Position of catalyst during growth decides which growth mechanism is on. If catalyst particle stays on substrate, it is called root-growth; if it raises with CNT, it is called tip-growth [27,32]. Schematic view of both tip-growth and root-growth is shown in Figure 1.5 [32]. Growth of CNT continues as long as carbon is fed unless amorphous carbon occurs on tip. Although, catalyst particle can heal such defect [33]. Due to that, tip-growth is a desirable mechanism to achieve longer CNTs.

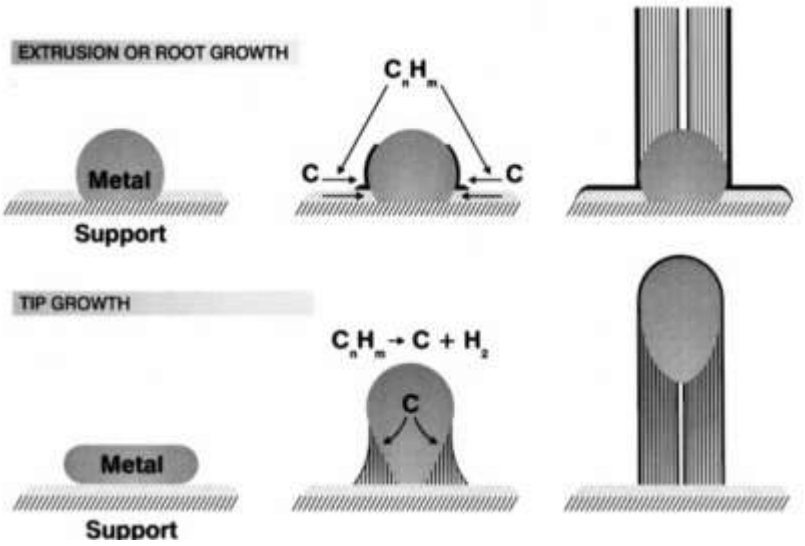

Figure 1.5. Schematic image of tip and root growth

According to these studies, most important parameters of CVD process that effect the growth have been discovered and can be listed as

- catalyst type [34],
- catalyst thickness [35]
- working temperature [24].

This wide variety of growth parameters opens new possible application to CNTs.

1.2.2 Carbon Nanotube/Polymer Nanocomposites

Carbon nanotubes (CNTs) possess high flexibility, high aspect ratio, high stiffness, low mass density, high electrical and thermal conductivity depending on chirality [3,36]. Combination of these properties of CNTs that makes them the ideal reinforcing agent for many different applications [37,38]. First, Ajayan et al. reported that CNTs using as reinforcing agent improve the mechanical behavior of polymer matrix [39]. Although they are considered as new generation high performance reinforcing materials, there are many challenges in the field high-performance CNT/polymer composites:

- using the highest aspect ratio CNTs,
- utilizing high volume fraction while maintaining CNT dispersion,
- synthesizing of high length CNTs with low waviness,
- developing technology for mass production.

Dispersion of CNTs is one of the big challenges compared to other fillers such as Al_2O_3, carbon fiber, graphite nanoplatelets (GNP) etc. because of its high aspect ratio and extremely large surface area [40] where van der Walls forces are dominating the behavior of distribution of CNTs. Three dimension distribution of micro-scale Al_2O_3 and carbon fiber fillers shows in Figure 1.6(a) and Figure 1.6(b) and homogeneous dispersion throughout polymer matrix can be clearly seen for micro-scale Al_2O_3 and carbon fiber fillers. On the other hand, when GNP and CNTs are filled into the same volume of matrix, dispersion of nano-scale fillers is harder than micro-scale fillers due to electrostatic interaction and van der Walls force as schematically represented in Figure 1.6(c) and Figure 1.6(d). Even if uniform dispersion is presented simple, it should be more complicated than schematics shown here [40].

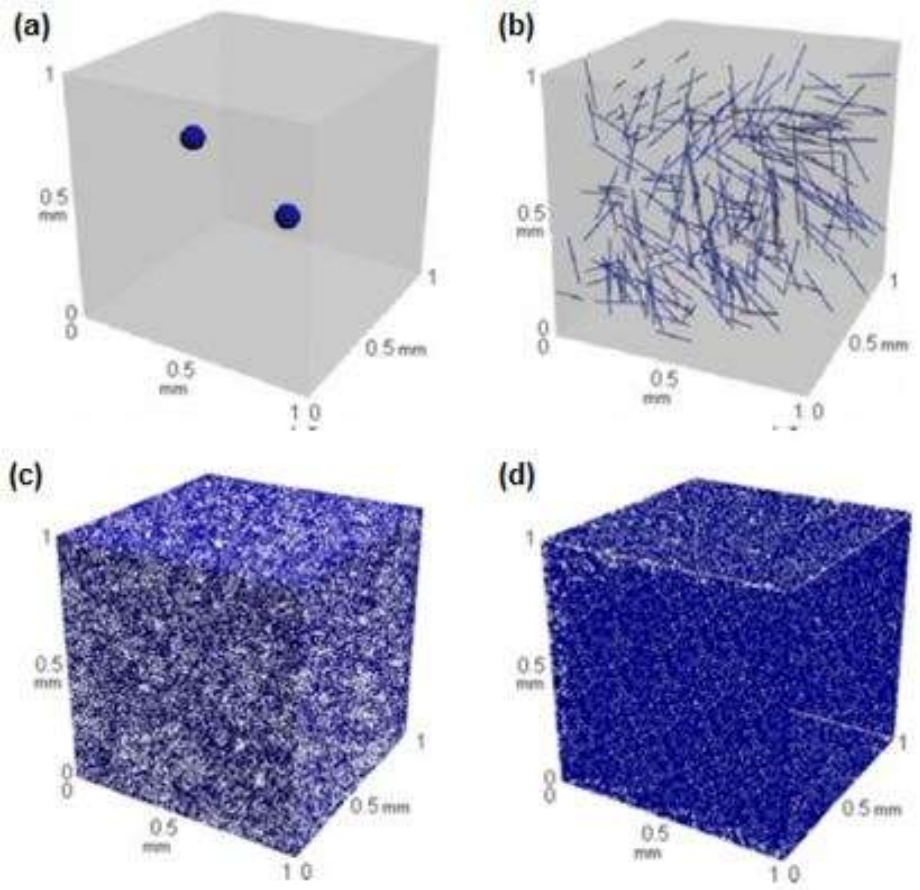

Figure 1.6 .Distribution micro- and nano-scale fillers of the same 0.1 vol. % in a reference volume of 1mm3 (a) Al2O3,, (b) Carbon fiber, (c) Graphite nanoplatelets (GNP), (d) CNTs)

Aim of many researchers has been directly fabricating of CNT/polymer nanocomposites without any functionalization to avoid additional steps in processing [38]. Since CNTs have huge aspect ratio (>1000) and large specific surface area, they tends to agglomerate into polymer matrix. Therefore, basic dispersion methods such as ultrasonication, calendaring, ball milling, high shear mixing can be employed to avoid agglomeration in polymer matrix [38]. Allaoui et al. fabricated nanacomposites using synthesized CNTs by CVD method. First, CNTs dispersed in methanol solution with magnetic stirring and after evaporation of methanol, CNT powder was directly filled in epoxy resin Bisphenol A/aromatic hardener mixture. Then, it was injected into mould after manual stirring. The mechanical properties of composites and neat resin is shown in Table 1.2. Even small quantity addition of CNTs can enhance the mechanical behavior of low modulus polymer resin as shown in Table 1.2 [41].

Table 1.2. Young modulus and stresses at different strain levels

CNT wt.%	Young's modulus (MPa)	Yield strength $\sigma_{0.2\%}$ (MPa)	$\sigma_{10\%}$ (MPa)
0	E_0=118	1	4
1	236 (2* E_0)	3	8
4	465(3.9* E_0)	6	10

Although CNTs improve physical properties of composites, they do not show CNTs full reinforcing capability for structural requirements in PNCs [42]. For this reason, vertically aligned carbon nanotubes (VA-CNTs) synthesized by CCVD at high temperature can be employed to fabricate structural composite as micro-fiber since they can be synthesized in a preferential orientation with high quality [43]. Ci et al. fabricated CNT-PDMS nanocomposites by an infiltration process. Millimeter long CNT (~3.5mm) array were synthesized on solid substrate by xylene-ferrecene CVD method. The infiltration process was performed at 1 Torr for 3h to remove bubbler. Then, composites were cured at 100°C. Mechanical tests were performed at Instron 5843 testing machine to compare mechanical behavior of pristine CNT, neat PDMS, oriented CNT-PDMS for longitudinal and transverse axes and randomly oriented CNT-PDMS nanocomposites represented in Figure 1.7 [44].

According to test results, continuous CNT composite exhibits drastic increase in stiffness compared to pure PDMS. While composite has 18.87 MPa longitudinal modulus between 0 to 8% strain, pure PDMS shows 2.63 MPa. On the other hand, modulus of pristine CNT is equal to 0.55 MPa. This is remarkable 600% and 3300% increase in longitudinal modulus compared with pure PDMS and pristine CNT (see Figure 1.8) [44].

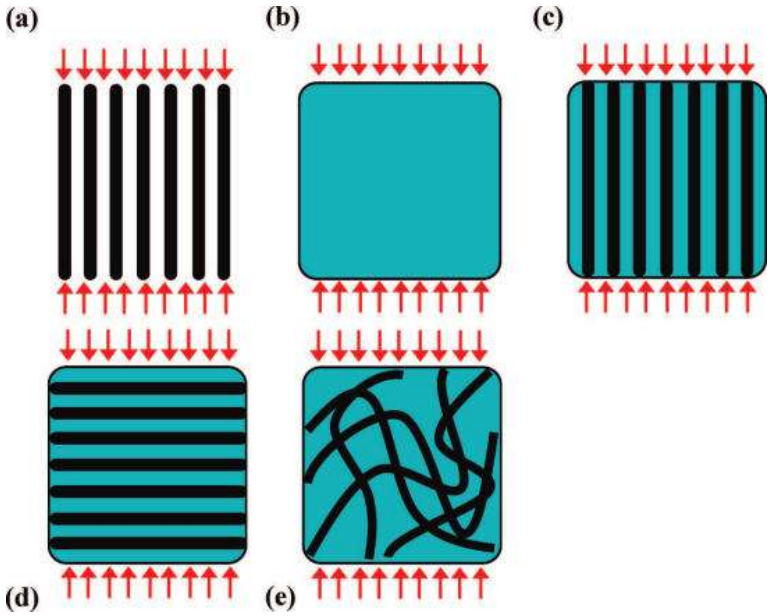

Figure 1.7. Schematics for different materials under compression (a) CNT forest, (b) pure PDMS, (c) continuous CNT-PDMS nanocomposites (longitudinal composites), (d) continuous CNT-PDMS nanocomposites (transverse composite), (e) randomly oriented CNT-PDMS nanocomposite

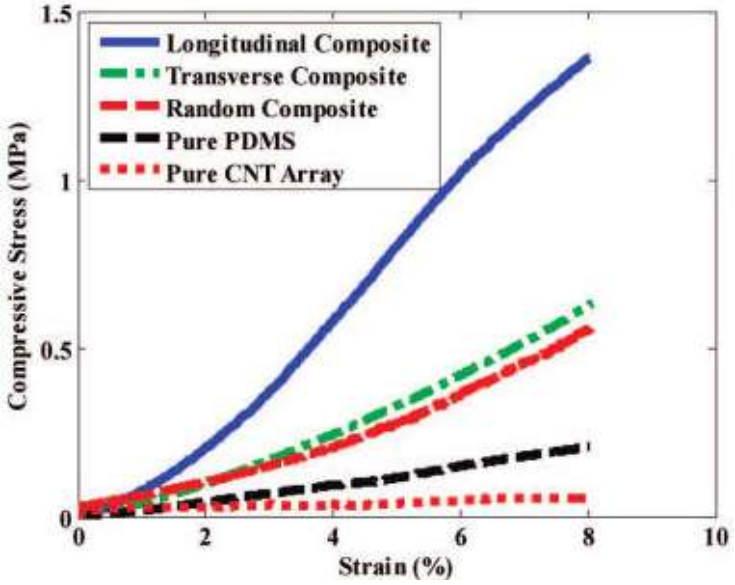

Figure 1.8. Monotonic stress-strain characterization of pure CNT array, pure PDMS, randomly oriented CNT-PDMS, and continuous CNT-PDMS nanocomposites for longitudinal and transverse axes

Some researchers investigated full-elastic behavior of aligned CNT-PDMS by using dynamic mechanical analysis (DMA) and tensile mechanical testing. They synthesized aligned CNT (A-CNT) by CCVD method with high quality. PDMS (Sylgard 184 Dow Corning Corp.) composes of base elastomer and curing agent. The base and curing

agent were mixed at 10:1 weight ratio. Then, mixture was waited at vacuum chamber for 15 min to remove bubbles. After A-CNT embedded with uncured PDMS, composite cured at 85°C for 30 min. Fabrication steps were shown in Figure 1.9 [42].

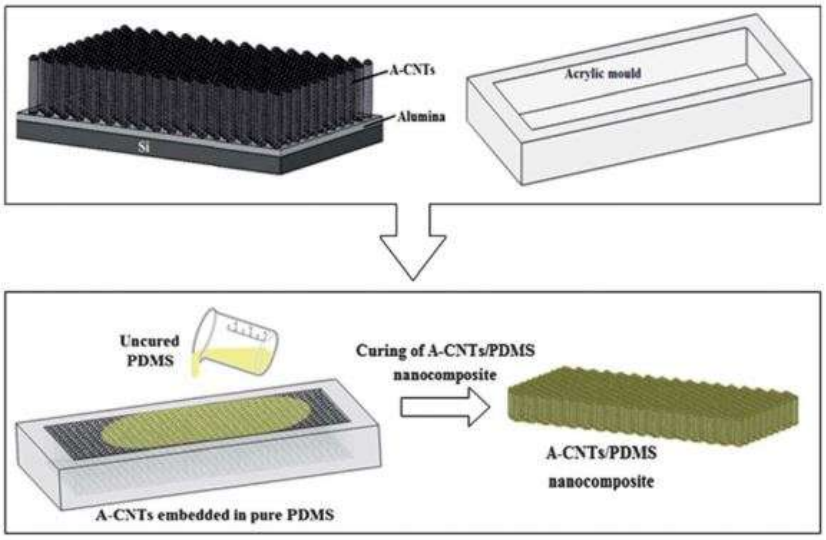

Figure 1.9: Fabrication process flow for A-CNT PDMS nanocomposite

Morphological characterization of A-CNT was achieved to observe alignment of CNT by using scanning electron microscopy. CNT alignment axis can be easily shown in Figure 1.10 [42].

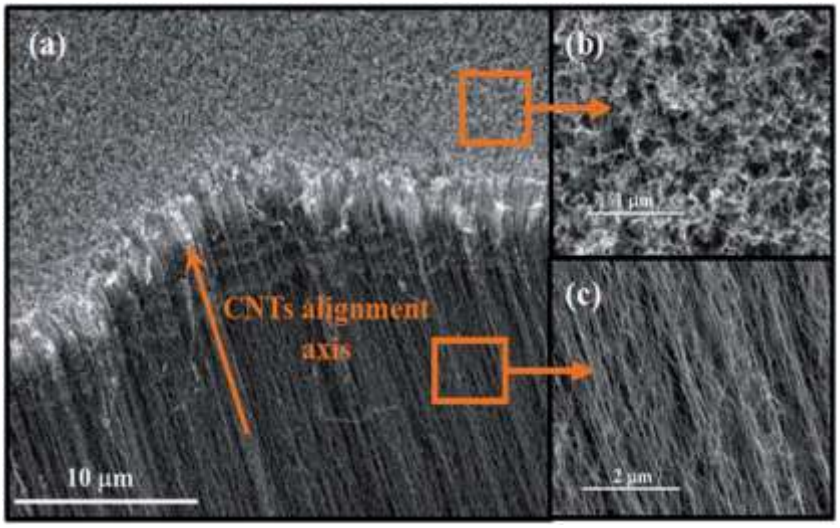

Figure 1.10. SEM image of A-CNT (b) and (c) are magnified region of (a)

An Instron 4505 mechanical testing machine was used to conduct tensile test of pure PDMS and nanocomposites. Strain measurement by optical extensometer was performed during mechanical tests. The stress-strain curves are presented in Figure 1.11 [42].

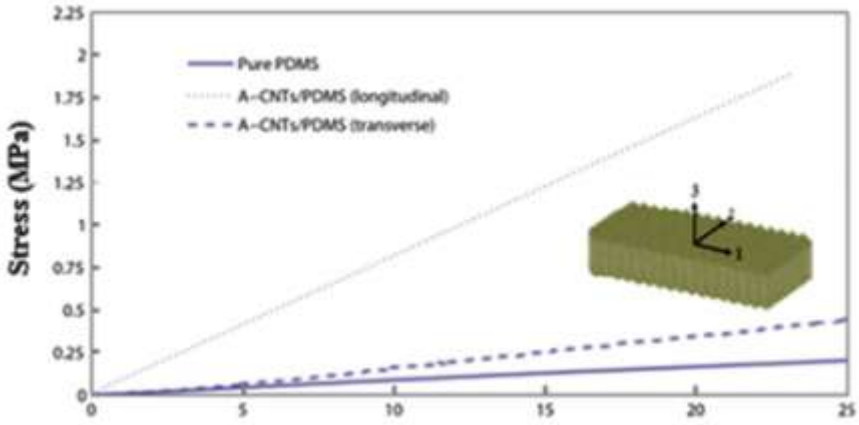

Figure 1.11. Representative stress-strain curves of pure PDMD and A-CNT/PDMS nanocomposites in longitudinal and transverse directions

Dynamic mechanical analysis method was used to obtain shear modulus as a function of frequency for both pure PDMS and A-CNT/PDMS nanocomposites at isothermal temperature. Figure 1.12. shows storage modulus and tan-delta curves of pure PDMS and A-CNT/PDMS nanocomposite to determine shear modulus [42].

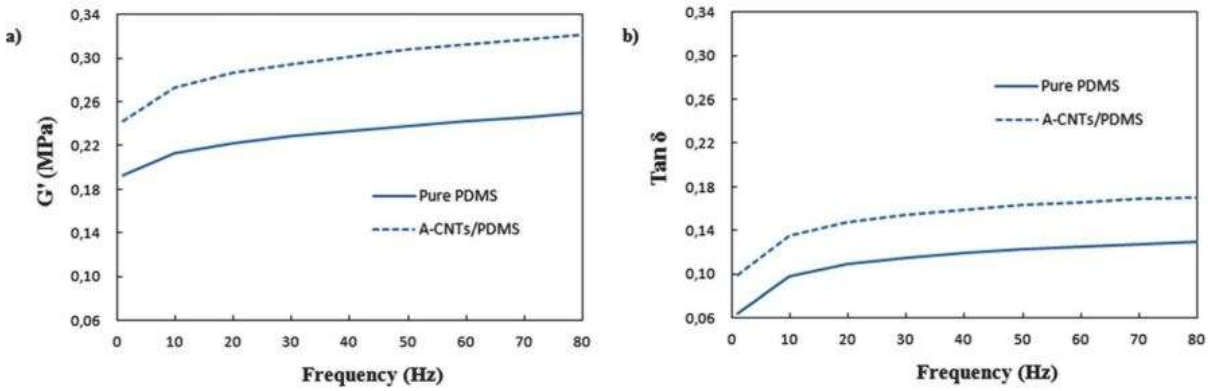

Figure 1.12. For pure PDMS and A-CNT/PDMS (a) storage modulus versus frequency, (b) tan-delta versus frequency

Wardle et al. achieved high-volume fraction CNT/nanocomposites with thermoset epoxies and they characterized nanocomposites by SEM at different magnifications. Normally, CNT can be synthesized with ~1%vol. fraction. CNT forests densified from 1%vol to 8 and 10%vol. to fabricate high volume fraction CNT/polymer nanocomposites. Optical photo, illustration and SEM images with different magnifications of CNT forests show in Figure 1.13. According to SEM images, CNT forest preserve alignment after mechanical densification [45].

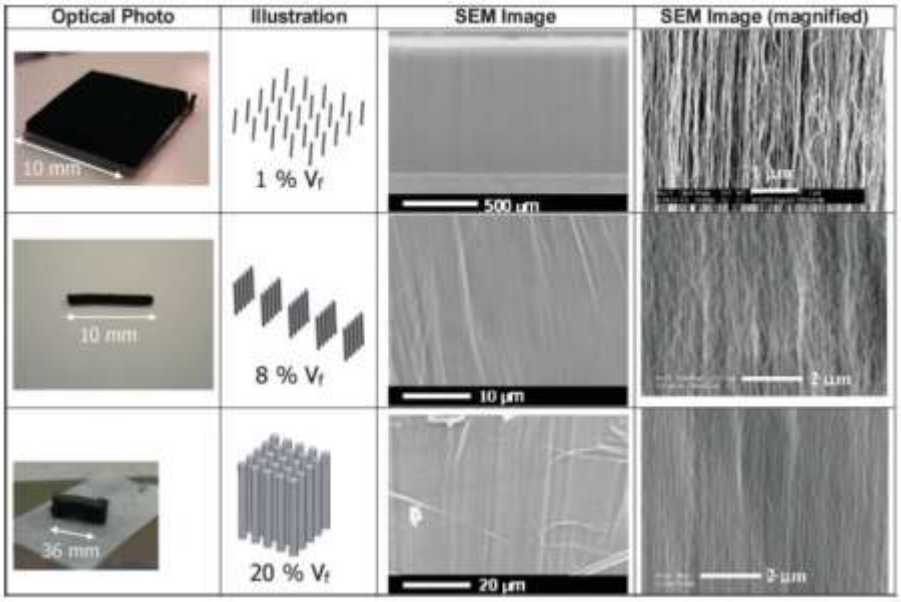

Figure 1.13. Aligned CNT volume fraction from mechanical densification of ca. 1mm tall CNT forests at 1% (as-grown), 8% (uniaxial densified), 20% (biaxial densified)

To produce high quality PNCs, viscosity of polymer and inter-tubular distance of CNT forest is crucial. In this work, thermosets that had been used as matrix material was pre-heated and filtered to lower viscosity. Effect of viscosity is shown in Table 1.3 [45].

Table 1.3: Thermoset epoxy characterization.

Epoxy	Brand	Usual application	Temperature during wetting (°C)	Viscosity at wetting temp. (cP)	Cure cycle
VRM34	Hexcel	Aerospace-grade advanced composites	90	12	1h/160°C 3h/180°C
RTM&	Hexcel	Aerospace-grade advanced composites	90	33	1h/160°C 3h/180°C
SU-8 2002	Microchem	Microfabrication	65	8	Prebake:5min/60 °C Exposure:UV light for 1 min Postbake:5min/90°C Hardbake: 30min/130°C

Moreover, SEM images of CNT/epoxy nanocomposites had been taken to check voids that may occur during production and the effect of densification on inter-tubular distance. SEM images are shown in Figure 1.14 [45].

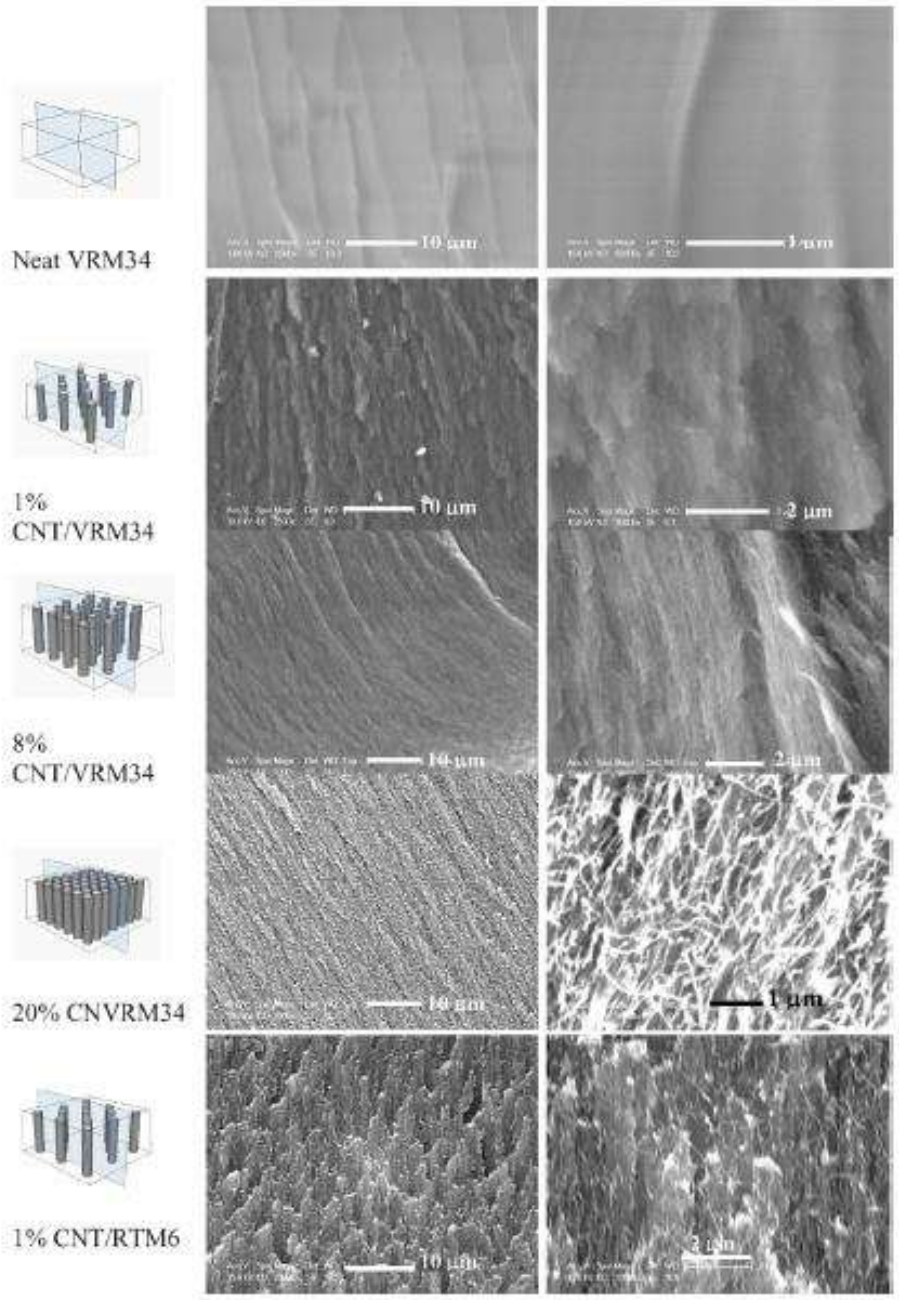

Figure 1.14. SEM images of PNC with various volume fraction

CNT/Polymer nanocomposites (PNCs) can also be classified by orientation of CNTs in composite. Randomly oriented CNT reinforced PNCs are the most common type of work in this field since it is relatively easy to produce and effective [46]. Biggest

challenge for this type of PNCs is the dispersion of CNTs. Due to Van Der Waals forces in between CNTs, they tend to stay together which causes agglomeration of them. By applying effective process technique, good distribution and dispersion is aimed in all PNC studies.

Melt blending is one of the most common methods to fabricate randomly oriented PNCs. Method is based on dispersion CNTs in polymer matrices at high temperatures. Therefore, the main force to disperse CNTs is shear forces caused by viscosity of molten polymer. Due to high viscosity, dispersion and amount of CNT that can be dispersed in matrix are relatively low. On the other hand, melt blending method is very successful with industrial plastics such as polycarbonate, polypropylene, nylon-6 etc. [35–38]

Another method to fabricate randomly oriented PNCs is by solution blending. In this method dispersed CNTs are mixed with a polymer at room temperature. This method is the simplest one to fabricate PNCs. Unlike melt blending, CNTs are dispersed in their own solvent; therefore, dispersion becomes more efficient. However, due to lack of dispersing forces, a powerful string step such as ultrasonication is needed in this method. This step is very critical for properties of final product since CNTs can be broken down during string which may cause decrease in aspect ratio. Nevertheless, variety of polymers as matrix material and surfactants to disperse CNTs, lots of possible fabrication variations can be obtain with respect to aimed properties [39–41].

The last main method to fabricate randomly oriented PNCs is by in-situ polymerization. In this method CNTs are dispersed in monomer and then CNT containing monomers polymerizes and at the end of polymerization, PNCs are obtained. Main advantage of this method is as it enables covalent bonding between CNTs and matrix material which supports the load transfer from matrix to CNT. On the other hand, adding CNTs into monomer increases viscosity of solution which limits the amount of CNTs that can be dispersed in monomer [42,43].

As a result of ability to produce A-CNTs, oriented PNCs are taken attention instantly since they may satisfy one of the fundamental requirements of good reinforcement which is the preferential alignment. One of the first studies have been done on oriented PNCs was done by Ajayan et. al [39]. The main aim of this work was producing a nanocomposite; mechanical measurements were not performed on these samples. When

aligned CNTs are considered as mechanical reinforcement material, volume fraction (V_f) of CNTs in matrix became important since rate of the increase of Young's modulus depend on this fraction. In work of Coleman et al., rate of Young's modulus increase is published as 18 GPa [56]. One of the first mechanical test demonstrated work has been done by Schadler et al. [57]. In this work, compression test had been applied on CNT/epoxy nanocomposite, and better results are obtained than tension test (rate of 26 GPa).

Therefore, steps to increase the of CNTs used during nanocomposite fabrication is an ongoing study in the literature, as well. Knock-down of CNTs is one of the most commonly used methods to achieve higher volume fraction; moreover, it also helps to align CNTs [58]. Bradford and co-workers published a novel way to produce oriented CNT containing polymer composites (PNCs) with high volume fraction for mechanical purposes [59]. In this work, VA-CNT forests are synthesized by CCVD and knocked-down with angular pressure. As a result, they have obtained buckypaper mode of compressed and oriented CNTs. With using these buckypapers, PNCs with volume fraction of 27% and tension tests are done on these samples. They achieved Young's modulus of 21 GPa.

1.3 Problem Definition and Motivation

As mentioned in previous parts, there are many requirements to make a polymer nanocomposite (PNC) efficient and successful. These requirements might be understood better by using mathematical models that are used to determine the quality of conventional composites such as fiber reinforced composites.

The most simple but one of the most beneficial model to explain mechanical behavior of composites is rule of mixture model [60].

$$\gamma_c = (\gamma_f - \gamma_m)V_f + \gamma_m \tag{1.1}$$

Where, γ_c is tensile strength modules of composite, γ_f is tensile module of fibre, γ_m is matrix modules and V_f is fibre volume fraction. However, this model is not valid for short fiber case; since, loads are carried by load transfer to fibers and short fibers can

carry load less efficiently. In order to make this model more convenient for short fiber cases, Cox [61] improved this model to;

$$\gamma_c = (\eta_l \gamma_f - \gamma_m) V_f + \gamma_m \tag{1.2}$$

Where η_l is the length efficiency factor which is described by [62];

$$\eta_l = 1 - \left(\tanh\left(\frac{a.l}{D}\right)\right) x \frac{D}{a.l} \tag{1.3}$$

With,

$$a = \sqrt{\frac{-3\gamma_m}{2\gamma_f \ln(V_f)}} \tag{1.4}$$

Another common model is developed by Halpin and Tsai [63]. For aligned fiber composites, the Halpin-Tsai model gives the modulus to be;

$$\gamma_c = \gamma_m \, x \, \frac{1 + \tau \eta V_f}{1 - \eta V_f} \tag{1.5}$$

Where,

$$\tau = \frac{2l}{D} \tag{1.6}$$

And,

$$\eta = \frac{\frac{\gamma_f}{\gamma_m} - 1}{\frac{\gamma_f}{\gamma_m} + 1} \tag{1.7}$$

The Halpin–Tsai equation is known to fit some data very well at low volume fractions but to underestimate stiffness at high volume fraction.

Therefore, according to rule of mixture model and Halphin-Tsai model, main requirements to achieve effective reinforcement can be listed as high aspect ratio, high fiber modulus, good alignment, high volume fraction and efficient load transfer [64].

Choosing vertically aligned carbon nanotube (VA-CNT) forests as reinforcement material satisfies the high fiber modulus and high aspect ratio requirements since CNTs are tubular material whereas diameters are in nanometer scale and lengths are in millimeter scale, and have great mechanical properties; however, to achieve the potential of CNTs in VA-CNT forests, forests must be synthesized with highest carbonization level [65]. Due to that, catalyst chemical vapor deposition (CCVD) method has been chosen to fabricate CNTs and process has been optimized to obtain highest graphitization level possible [66].

One other benefit of using VA-CNT as an additive is VA-CNTs are self-aligned. Although, direction of alignment of CNTs might not be the desired direction for every case. Therefore, knock-down process has been applied to VA-CNT forests to obtain desired orientation. In fact, this step also helped to enhance the volume fraction of reinforcement in nanocomposite.

Besides of these requirements, efficient load transfer is the most critical one for PNCs. In order to maximize the mechanical behavior of nanocomposite, external loads applied on system must be efficiently transferred to CNTs since tension modulus of CNTs are greater than tension modulus of matrix material ($\gamma_f > \gamma_m$) [57]. This transfer mechanism directly depends on the interaction between CNT and matrix material, which is epoxy for our study. To enhance this interaction, a solution to adhesion as ozone treatment with various parameters are applied on CNTs.

CHAPTER 2 Experimental Methods

2.1 Synthesis of Vertically Aligned Carbon Nanotube Forest by Thermal Chemical Vapor Deposition

There are several methods to synthesis vertically aligned carbon nanotubes (VA-CNTs) such as arc discharge, laser ablation and chemical vapor deposition. Each of these methods has their own advantages and disadvantages. End product of all of these techniques contains different structure of carbon including CNTs; however, unlike other techniques CVD has high yields of obtaining CNT form. Hence, purification or another extra step is needed which makes CVD process convenient and efficient for applications[42,43,24].

In CVD process for VA-CNT growth, there must be catalysis, temperature and carbon source. Transition metals such as iron, molybdenum, nickel are good candidates as catalysis; since, they ease carbon diffusion in their structure and have low probability of occurring carbides [34]. As carbon source of process, any precursor that can decompose to free carbon and can be fed to the system can be chosen. Methane, ethylene and butane in gas phase are some of the commonly used carbon sources [44,26]. Generated free carbon is adsorbed on catalysis, which acts as nucleation site, and keeps growing as long as carbon source is fed.

2.1.1 Substrate Fabrication

VA-CNT growth process happens at high temperatures; therefore, a solid and durable to high temperature substrate is required to coat catalysis. Bare silicon wafer with <100> orientation is chosen as substrate since it satisfies the requirements.

In this study, various production methods of similar catalysis structure coating on substrate are studied [71]. In the first catalysis structure, which will be referred as reference structure, before catalysis coating, silicon wafer is coated with 300 nm thick silicon dioxide (SiO_2) layer by plasma enhanced chemical vapor deposition (PE-CVD). The reason of coating this layer is avoiding the silicide formation between silicon wafer and the catalysis at high process temperature [71]. In this step, Oxford Instrument PE-CVD is employed. Parameters of PE-CVD process used in formation of SiO_2 is shown in Table 2.1.

Table 2.1. Parameters of PE-CVD process

Parameter	Values
SiH_4	170 sccm
N_2O	710 sccm
Pressure	1000 mTorr
RF	20W
Temperature	300°C
Time	4 min

Figure 2.1. Oxford Instrument PE-CVD

On 300nm SiO_2 layer, 10 nm Alumina (Al_2O_3) and 2 nm iron (Fe) layers are coated respectively with e-beam evaporator [46–48]. Torr International, Inc. e-beam evaporator is used in this step. Al_2O_3 layer acts like a barrier between Fe and SiO_2; moreover, it affects CNT morphology, growth rate and orientation [48,49]. Then, iron layer is coated on alumina layer as catalysis layer. To avoid roughness as much as possible that may have been occurred by evaporation, coating rates are chosen as 0.1-0.2 Å/s for iron and 0.3-0.4 Å/s for alumina.

Figure 2.2. Torr e-beam evaporator used for alumina and iron layer coating

In the first catalysis structure, consistency issues have been experienced; in order to solve this problem, coating technique has been changed from e-beam evaporation to sputter for iron [71]. This three stepped structure will be referred as sputter in following parts. The reason behind using sputter technique is magnetic properties of iron. Since iron is a ferromagnetic material and e-beam evaporator generates magnetic field, quality of iron layer coating has been suspected. Argon (Ar) plasma has been used for sputter deposition. Parameters that have been used is shown in Table 2.2.

Table 2.2. Parameters used for sputter coating

Parameter	Values
Ar flow	35 sccm
Applied power (DC)	200 W
Pressure	10 mTorr
Gate Valve	360
Time	30 s

To obtain an identical structure with reference structure, iron layer have to be 2 nm; however, with the parameters above 4.9 nm thick iron layer is obtain. To decrease thickness, various coating times have been tried. Coating time is decreased to 10

seconds from 30 seconds by 5 seconds. Thickness values are represented by time is shown in Figure 2.3. Thicknesses of coatings are measured with elipsometer.

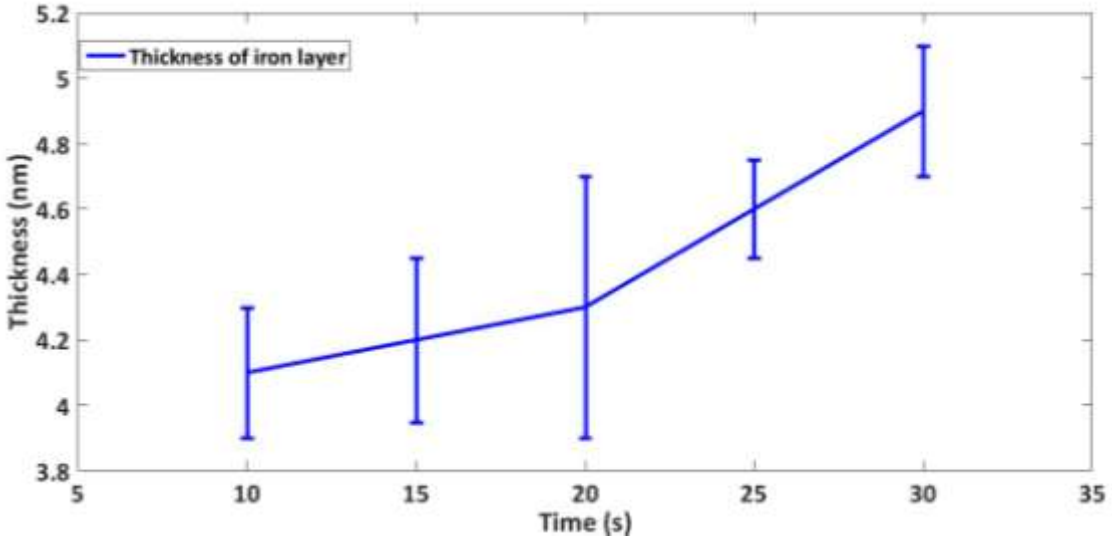

Figure 2.3. Sputtered coating thickness change by time

As shown in Figure 2.3, by adjusting time of coating process, desired coating thickness could not been obtained, and further process optimization is needed for sputter. Instead of making this three stepped production more complex, new structure, which will be referred as oxide-free, have been developed. In this structure, silicon dioxide layer has been removed and e-beam evaporation step kept same in reference structure. By this change of structure, substrate preparation has become one step process and consistent.

Finally, to show the effect of silicon dioxide layer, commercially available <100> oriented silicon wafer with 300 nm thermal oxide layer has been coated with alumina/iron layers by e-beam evaporator. This structure will be referred as thermal in further parts.

2.1.2 Nucleation and Growth

To synthesis CNTs, catalyst chemical vapor deposition (CCVD) has been used. As CCVD system, three zoned furnace with 4.5 cm inner diameter quartz tube and helium

(He), hydrogen (H_2) and ethylene (C_2H_4) gases are used [31]. CCVD process has five main steps which are purge, nucleation, growth, delamination and cooling.

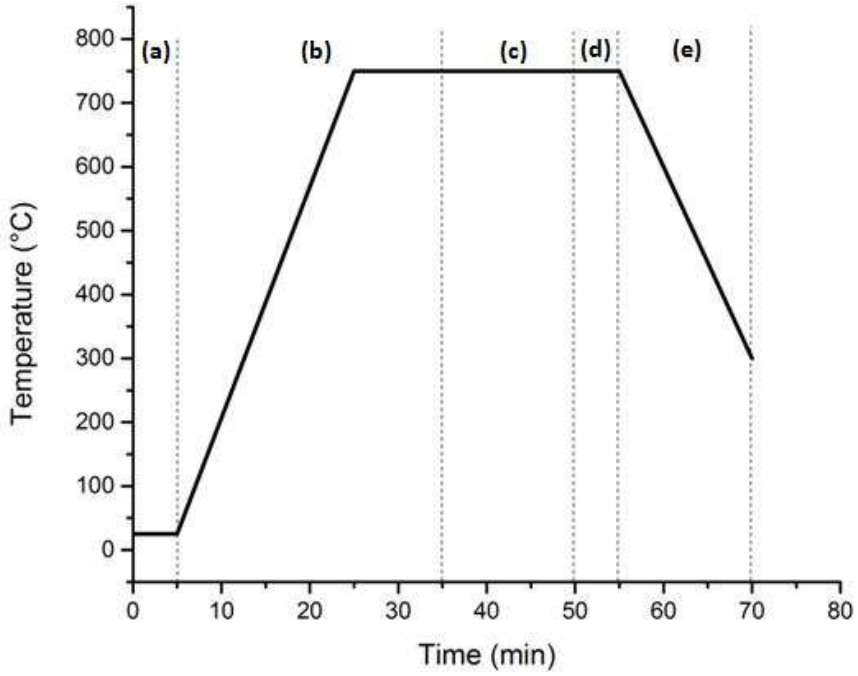

Figure 2.4. Steps of CCVD process a) Purging b) Nucleation c) Growth d) Delamination e) Cooling

Before starting the synthesis, catalyst coated silicon wafer with desired dimensions is placed to thermally stable zone of furnace, then, system is closed and connected to gases. Process starts with purging step. In this step, system is fed with He at room temperature to remove oxygen (O_2) and to provide an inert reaction atmosphere. Then, system is heated up to 750 °C with 35 °C/min heating rate and stayed at that temperature for 15 minutes. Meanwhile, He and H_2 are fed to system. During this nucleation step, H_2 reduces iron oxide to iron and activates binding sites of catalyst to enable iron to adsorb carbon in growth step, and with temperature iron particles become liquid phase [33,50,28]. As mentioned in the vapor-liquid-solid model (VLS), this step has great impact on the structure of final CNTs [51,23]. After nucleation, growth step starts. In this step, He, H_2 and C_2H_4 are fed to system at 750 °C for 15 minutes. C_2H_4 is the carbon precursor of the process. At 750 °C, it breaks down to free carbon (C) in an inert atmosphere. Generated free carbon forms carbides with liquid metals on substrate. CNTs are grown when these carbide particles are supersaturated in carbon; therefore,

chosen metal for catalyst must be a solvent for carbon [78]. In this step, C_2H_4/H_2 ratio defines the rate of growth; due to that, partial pressure of these gases and process temperature have an important role on CNT structure. On right growth rate, CNTs can grow as long as carbon is fed unless the structure is closed by an amorphous carbon. At the end of growth step vertically aligned carbon nanotube (VA-CNT) forests are obtained. After this step, H_2/He mixture is sent to system at 750 °C to weaken the bonds between CNTs and iron. The purpose on that is removing CNT forest easily from substrate. This step is called as easy delamination process and is an optional application [27]. Afterwards system is left to cool-down to room temperature with presence of He. CCVD recipe used in this study is shown in Table 2.3.

Table 2.3. Recipe of VA-CNT growth

Steps	**He (sccm)**	**H_2 (sccm)**	**C_2H_4 (sccm)**	**Time (min)**	**Temperature (°C)**
Purge	1000	-	-	5	25
Nucleation	1500	1000	-	15	750
Growth	1000	600	400	15	750
Delamination	1000	500	-	1	750
Cooling	300	-	-	-	300

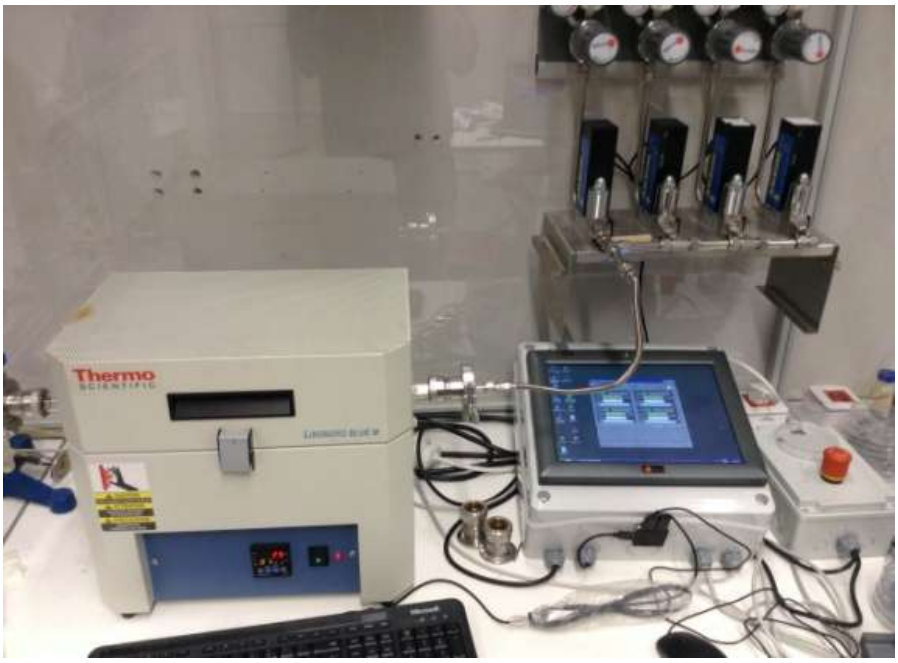

Figure 2.5. CCVD system used in VA-CNT forest synthesis

With optimizing the CCVD process, CNT lengths have been increased up to 1.4 mm. Before that, average length of CNTs were around 350 µm. Change in length is shown with scanning electron microscope images in Figure 2.6 and Figure 2.7.

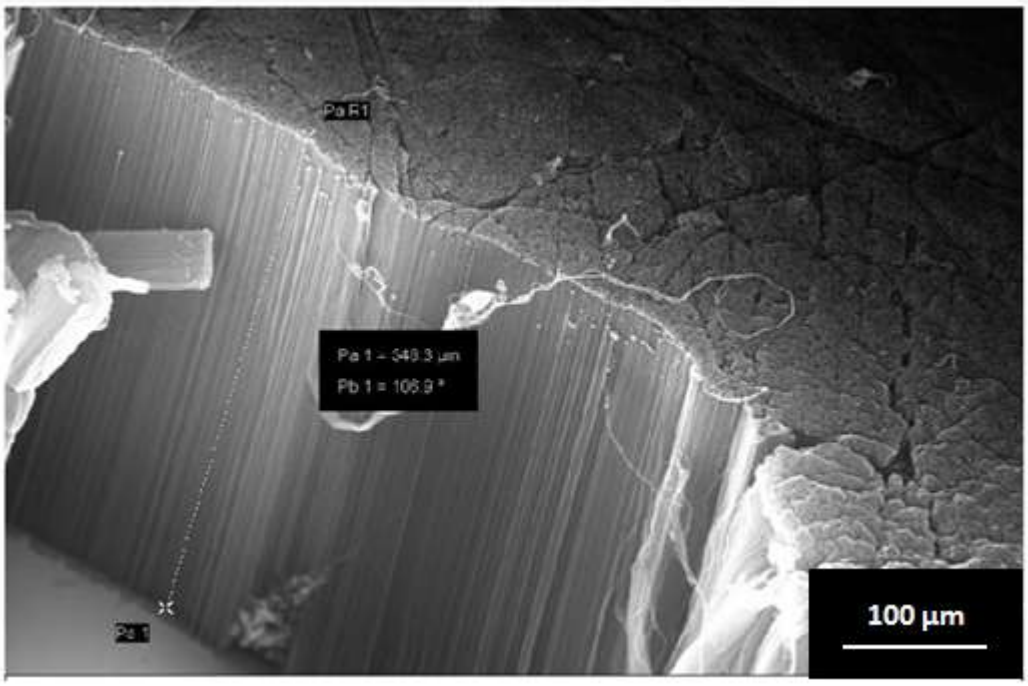

Figure 2.6. SEM image of VA-CNT forest before optimization

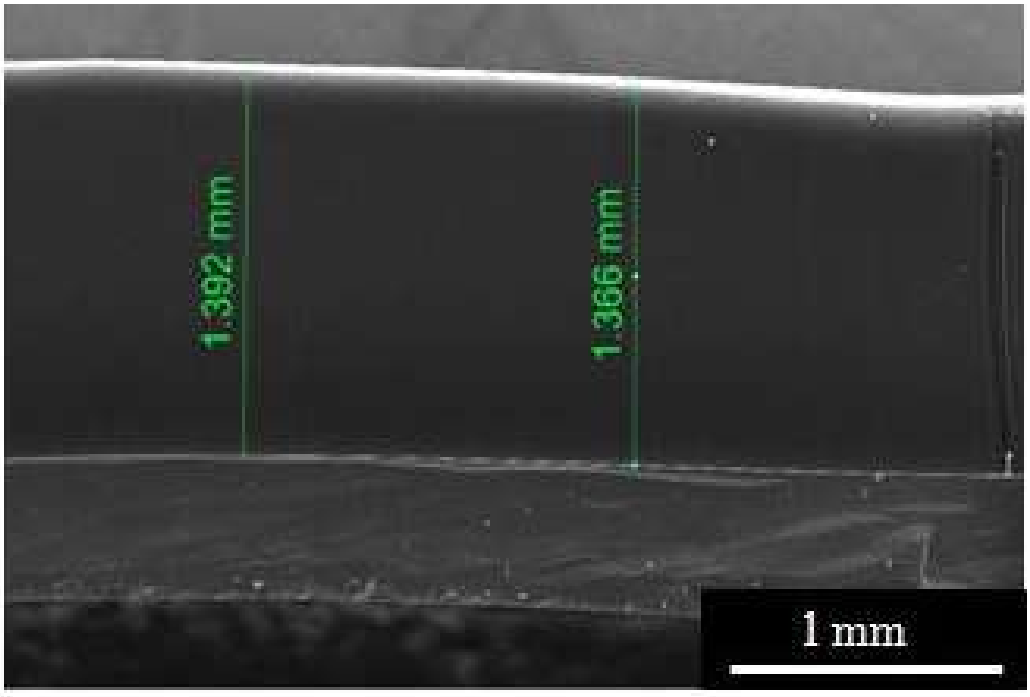

Figure 2.7. SEM image of VA-CNT forest after optimization

2.2 Fabrication of Carbon Nanotube/Epoxy Nanocomposites with Vacuum Infusion Method

CNT forests have been used as additives for epoxy matrix nanocomposites because of their high aspect ratio and tensile strength [37]. Vacuum infusion method has been used to fabricate nanocomposites. Unlike conventional vacuum infusion method, matrix material has been put in vacuum bag to increase volume fraction of CNTs. Schematic of vacuum infusion fabrication is shown in Figure 2.8.

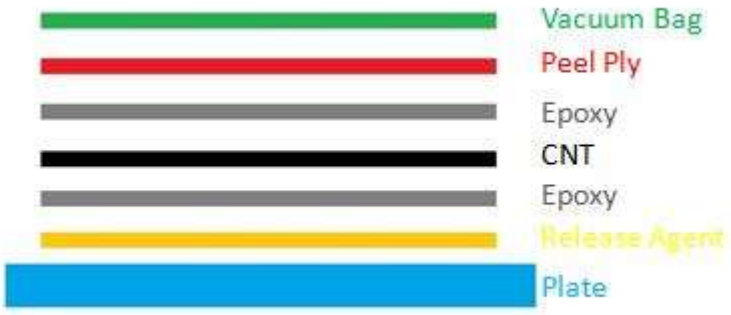

Figure 2.8. Schematic of vacuum infusion

As matrix material, epoxy in sheet form with 600 mPa.s viscosity and glass transition temperature (T_g) of 125 °C has been used, and as an additive material, oriented CNT forests have been used. To obtain oriented CNT forest, VA-CNT forests were knocked-down with a roller. CNTs can be treated with ozone (O_3) before knock-down process optionally. After knock-down, oriented CNTs were removed from substrate with help of a razor.

Figure 2.9. Preparation of oriented CNTs

2.2.1 Ozone Treatment

One of the most challenging problems of CNT/polymer nanocomposites is achieving good surface interaction between CNTs and matrix material. In this study, ozone treatment has been applied on VA-CNT forests to weaken interactions between CNTs and increase the wettability of CNTs by etching CNTs with reducing them to carbon monoxide and carbon dioxide (see Figure 2.10) in order to obtain better surface interaction with matrix material [79].

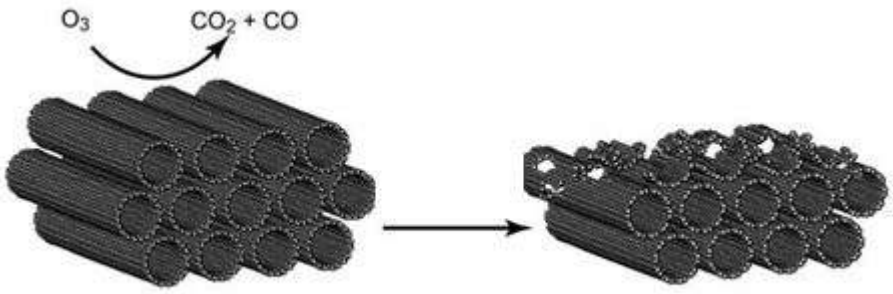

Figure 2.10. Mechanism of ozone etching of CNT

For this purpose, A2Z ozone generator has been employed. Synthesized VA-CNT forests on substrate have been put in a glass reactor and generated ozone has been sent to reactor with 3 L/min flow.

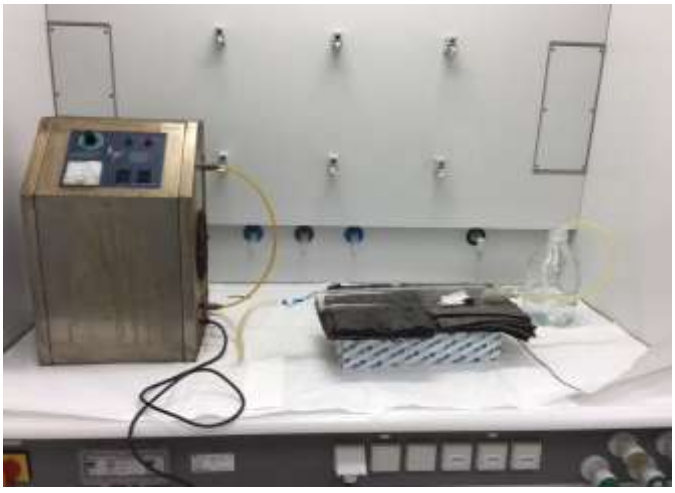

Figure 2.11. A2Z ozone generator and ozone treatment setup

2.2.2 Knock-Down Process

Knock-down process has a great impact on improving mechanical properties of nanocomposite. This step increases the volume fracture of CNTs in nanocomposite by stacking CNTs; moreover, it provides the alignment. VA-CNT forest on substrate is connected to a stable surface. Then, VA-CNTs are knocked-down by movement of roller in a certain direction. For our samples, CNTs are aligned through the long edge of samples. After knock-down process, oriented CNTs are removed from substrate with help of a razor [58].

PTFE roller with 0.5 cm diameter has been used for this work. Roller material is chosen as PTFE to avoid attachment of CNTs on roller, and diameter of roller is chosen as small as possible to avoid pressing the CNT forest [80].

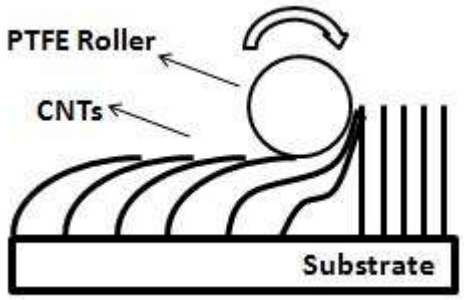

Figure 2.12. Schematic image of knock-down process

2.2.3 Preparation of Oriented Carbon Nanotube/Epoxy Nanocomposites

Polymer nanocomposite (PNC) fabrication starts after preparing oriented CNTs. First, a clean and smooth plate is bounded with silicon tape which defines the vacuum area. In this work, a piece of flat glass has been chosen as plate for vacuum infusion and bounded with silicon tape. Afterwards, silicon pipe where air will have been pumped out has been connected to one side of silicon tape. Glass plate with silicon tapes and pipe is shown in Figure 2.13.

Figure 2.13. Glass plate with silicon tapes and pipe

After area is bounded, removal agent, which is resistive to high temperatures, has been applied to surface of glass plate to remove PNC easily after process. Meanwhile, two pieces of epoxy sheets (CP002, purchased from C-M-P GMHB) are cut to 40 mm by 10 mm and placed on a piece of peel-ply. Peel-ply is a kind of textile which helps to remove PNC from vacuum bag and distributes epoxy on surface equally. Therefore, choosing peel-ply size as needed is important.

On top of two layers of epoxy sheet, prepared oriented CNTs are placed. These VA-CNT forests have been synthesized on 33 mm by 8 mm substrate because of the standard of the mechanical test (ASTM D4065). At the end, two layers of oriented CNTs are laminated between two layers of epoxy sheets on the top and the bottom of PNC structure. Image of pre-cured PNC on peel-ply is shown in Figure 2.14.

Figure 2.14. Pre-cured PNC on peel-ply

Figure 2.15. Vacuumed PNCs

Prepare pre-cured PNCs with peel-ply are placed on glass substrate to get cured. Before curing step, whole system has been closed with a piece of high temperature resistive vacuum bag and vacuumed with help of an oil pump (shown in Figure 2.15). After leak control, vacuumed PNCs have been heated up to 135 °C and kept at that temperature for an hour.

At the end of one hour, system has been left to cool-down. PNCs have been removed when temperature is dropped to room temperature. Final products are shown in Figure 2.16.

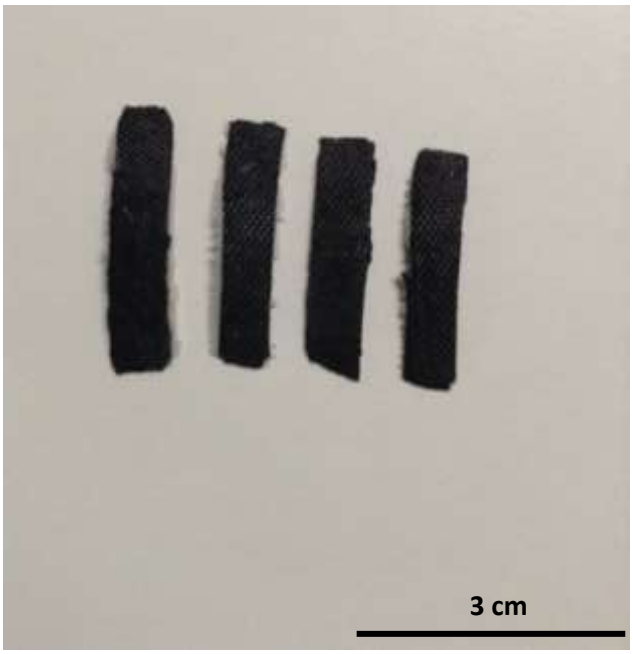

Figure 2.16. Final products

CHAPTER 3 Characterization and Analysis

3.1 Morphological Characterization of Vertically Aligned Carbon Nanotubes

CNTs can have various structural, mechanical and conductivity properties according to changes on their production and after-production steps. Hence, using proper characterization method to understand limitations and benefits of synthesized CNTs accurately is necessary. RAMAN spectroscopy, thermogravimetric analysis (TGA) and scanning electron microscopy (SEM) are the most commonly used characterization methods to analyze CNTs [78].

3.1.1 Thermal Properties

Thermogravimetric analysis (TGA) is one of the most commonly used characterization technique to determine quality of CNTs. Using TGA also enables to estimate a degree of purity and the resistance to oxidation of CNTs. Thus, the percentage of undesired materials such as support material and catalyst particles can be obtained quantitatively [50,57]. Also, it can be used for measurement of CNTs volume fraction into the polymer nanocomposites under nitrogen atmosphere [59]. TGA analysis were performed VACNT to identify the temperature of the maximum rate of the oxidation at TA Instrument SDT Q600 for this study.

Figure 3.1. TA Instrument SDT Q600

3.1.2 RAMAN Spectroscopy

Quality and purity of synthesized carbon nanotubes on lab-scale and mass-production must be measured with a powerful, non-destructive and fast method which is giving information about both structural and electronic properties of CNTs [58,59]. Since Raman spectroscopy provides all of these information, it is commonly used for carbon-based materials such as SWCNT, MWCNT, graphite, graphene etc. [84]. A low frequency peak (<500cm^{-1}), which is named as radial breathing mode (RBM), gives basic information about the tube diameter distribution in presence of SWCNTs [82]. In Raman shifts, a group of peaks around 1331 cm^{-1}, which is called D-band, is assigned to presence of the disorder in the CNT structure, 'G-band' is observed in 1584 cm^{-1}. This peak is a good measurement of graphitization of CNTs [85]. For this reason, ratio of intensities of G and D peaks that are measured by Raman Spectroscopy is an indicator of purity and quality of CNTs. Raman spectroscopy has been performed using Renishaw inVia reflex microscopy and spectroscopy with an excitation energy 2.32 eV and acquisition range from 100–3000 cm^{-1}.

Figure 3.2. Reinshaw inVia reflex Raman Spectroscopy

3.1.3 Morphological Properties

Scanning electron microscope (SEM) is a convenient method display nanomaterials since excited area can be decreased to nano-scale. Due to that, it is a good technique to investigate morphology of CNTs and determine the density of VA-CNT forest. Since CNTs are conductive materials, relatively high resolutions can be obtained. Therefore, inter-tubular distances, approximate tube diameter and waviness of CNTs can be calculated with a simple image processing [86].

3.2 Mechanical and Wetting Analysis of Carbon Nanotube/Epoxy Nanocomposite

3.2.1 Contact Angle Measurement

Contact angle measurement is a commonly used and a simple technique to evaluate the surface energy of materials and surfaces. Surface tensions of studied surfaces are defined related to water; due to that, results of measurements are named as hydrophobic or hydrophilic depend on angle between surface and water drop. A material or a surface is named hydrophilic if the contact angle is less than 90°, and between 90° and 150° it is hydrophobic and above 150° it is superhydrophobic [63,64].

This measurement provides information about wettability of material. Therefore, contact angle measurement technique is a good method to estimate interaction between CNTs and epoxy [89].

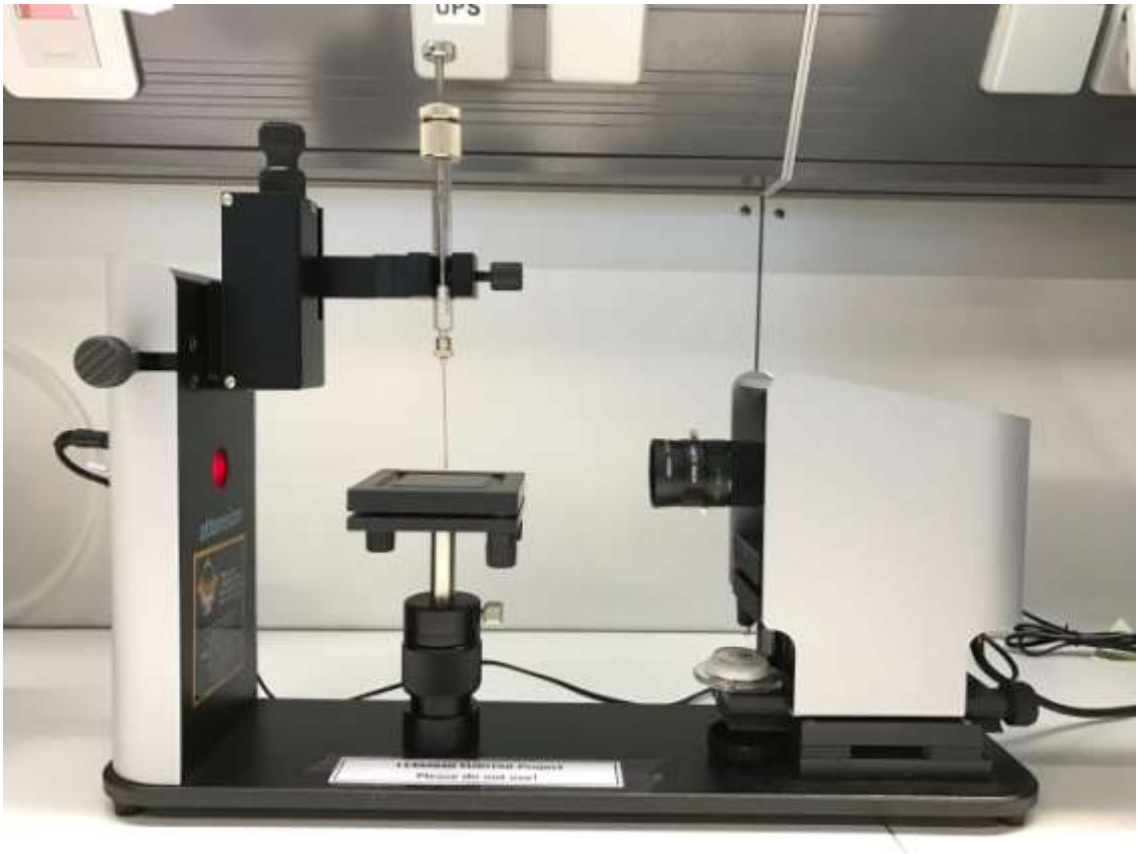

Figure 3.3. Contact angle measurement setup

3.2.2 Dynamical Mechanical Analysis

Traditional engineering structure deals with elastic solid and viscous liquid. Purely elastic materials are deformed in a proportion to the applied stress according to Hookean's Law (Figure 3.4.(a)). On the other hand, viscous liquids undergo irreversible deformation when applied stress and phase angle between stress and strain is equal to 90° (Figure 3.4. (b)). However, synthetic polymers, wood, human tissue as well as metals at high temperature display both elastic and viscous behavior named as 'viscoelastic' behavior under deformation. Phase angle between applied stress and strain is range from 0° to 90° as shown in Figure 3.4. (c). Therefore, most of researchers focus on the viscoelastic behavior of materials depending on time, temperature and frequency [90].

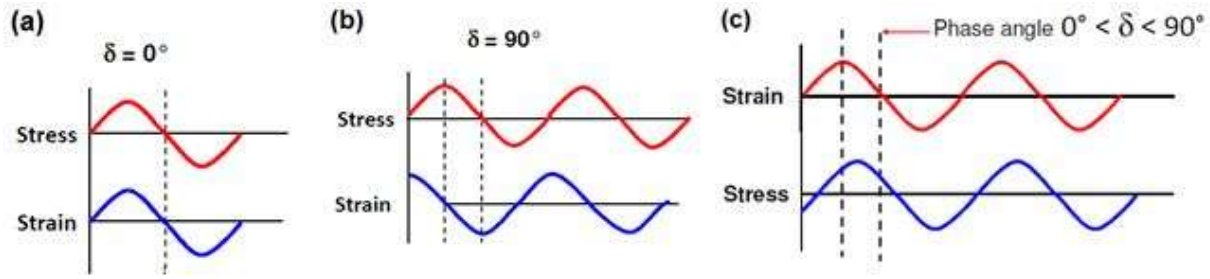

Figure 3.4. (a) Purely elastic response (Hookean solid), purely viscous response (Newtonian liquid), (c) viscoelastic material response

Since phase angle occurs between deformation and response, viscoelastic materials behaves both elastic and viscous. Due to this reason, two different modulus are defined for viscoelastic response. These are shown in details as below.

The elastic (storage) modulus (E′) is measurement of elasticity of material. It indicates the ability of the materials to store energy. It is calculated with,

$$E' = (stress/\text{strain})\cos\delta \tag{3.1}$$

The viscous (loss) modulus (E′′) is measurement of viscous characteristic of material. It shows the ability of the material to dissipate energy. It is calculated with,

$$E'' = (\text{stress}/strain)\sin\delta \tag{3.2}$$

Tan delta (δ) is a measure of damping ability of materials such as vibration. It is ratio of the loss modulus (E′′) to the storage modulus (E′) as;

$$\tan\delta = \frac{E''}{E'} \tag{3.3}$$

Dynamic mechanical analysis (DMA) method is a technique used for obtaining of static and dynamic properties of polymeric materials depending on temperature, time, frequency and strain [67–69]. For this reason, VACNT-PNCs fabricated with synthesized VACNT using with no treatment and ozone etching treatment tested with DMA to measure viscoelastic properties of PNCs at frequency sweep from 1 to 100 Hz using with tension film clamp such as illustrated with representative volume elements

(RVEs) for each loading state. All samples were tested at 50μm amplitude at room temperature by using TA Instrument Q800. Furthermore, static tests of VACNT-PNCs were achieved with tension-film clamp at room temperature. Overall samples were fabricated according to convenient dimension for ASTM D4065-12.

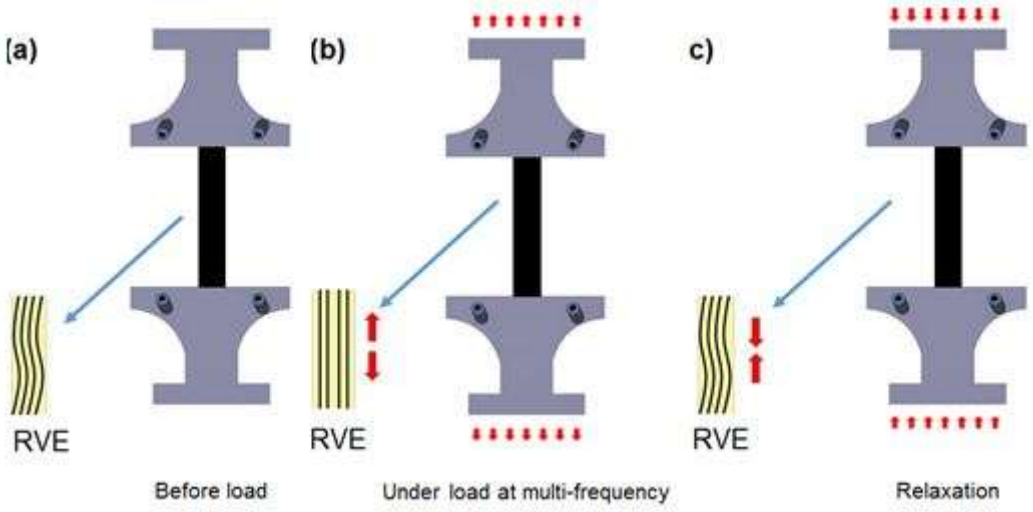

Figure 3.5.Illustrations of knock-down CNT/epoxy PNCs with representative volume elements (RVE) at tension-film mode at DMA (a) before load, (b) under load at multi-frequency range from 1-100 Hz, (c) after load

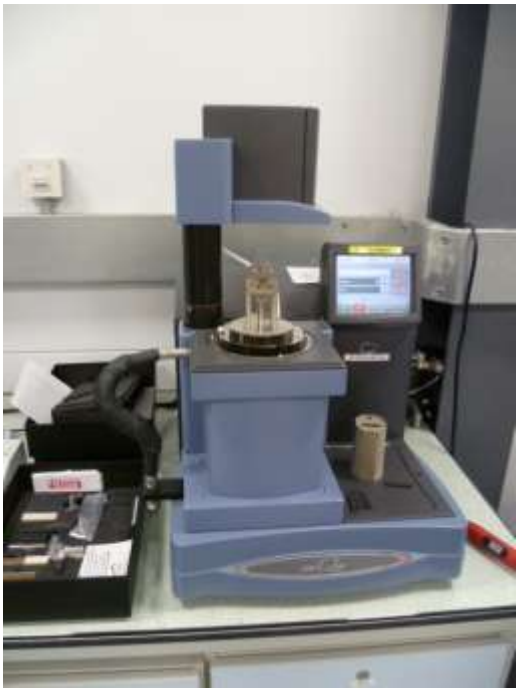

Figure 3.6. DMA setup used in tests

CHAPTER 4 Results and Discussion

4.1 Influence of Different Catalyst Structures on Carbon Nanotube Quality

In this part, effect of different catalyst structures on structural, morphological and mechanical properties of VA-CNT forest are analyzed and discussed. To do this investigation, VA-CNT forests are synthesized under same conditions on reference, sputter and oxide-free catalysis systems, which are mentioned in previous chapters, then thermal properties, qualities and morphologies of these CNTs are tested with Thermogravimetric Analysis (TGA), RAMAN spectroscopy and Scanning Electron Microscope (SEM).

4.1.1 Thermogravimetric Analysis Results

As mentioned in previous chapters, TGA is used to determine the quality and oxidation resistance of CNTs. Therefore, CNTs produced on different catalyst systems are tested on TGA up to 1000 °C under oxygen atmosphere. Since TGA measures the mass change respect to temperature, temperature where loss on mass starts, decomposition of CNT starts. Therefore, decomposition temperature is a sign of physical stability of CNT, in other words, it shows the thermal resistance of CNTs.

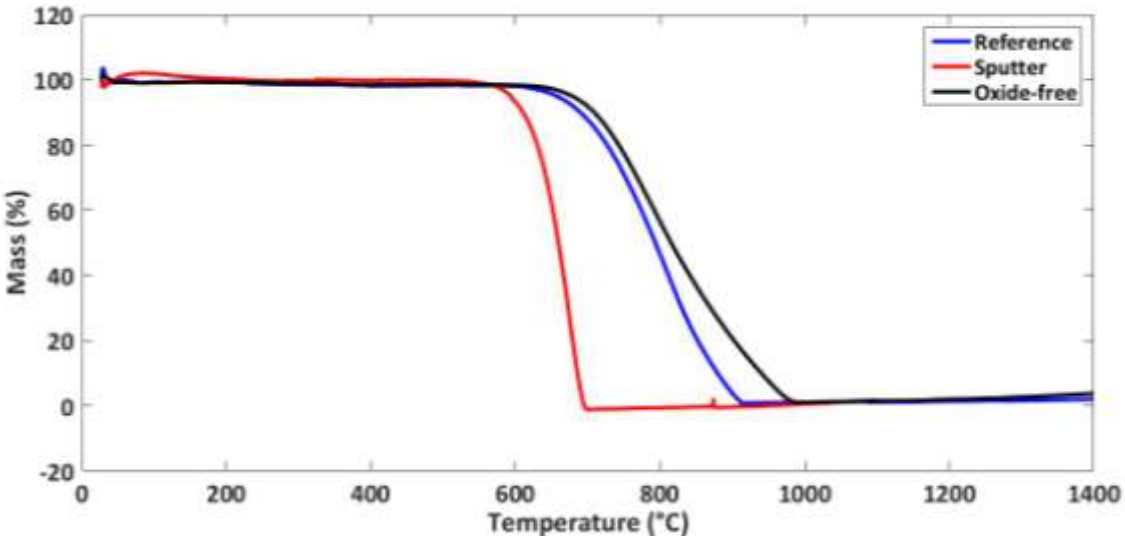

Figure 4.1. TGA curves of CNTs produced on different catalyst system

According to that, Figure 4.1 shows that CNTs grown on sputter catalyst system has the lowest decomposition temperature; although, CNTs grown on reference and oxide-free systems show similar TGA profiles. Therefore, we can predict that using oxide-free or reference catalyst system to synthesize VA-CNT forests for nanocomposite applications may provide a benefit.

Another thing that is used to evaluate CNT quality is rate of oxidation. To observe such parameter, rate of decomposition is plotted by taking first derivative of mass change curve respect to temperature. Minimum point of this curve tells where oxidation is fastest. Due to that, this value is wanted as low as possible.

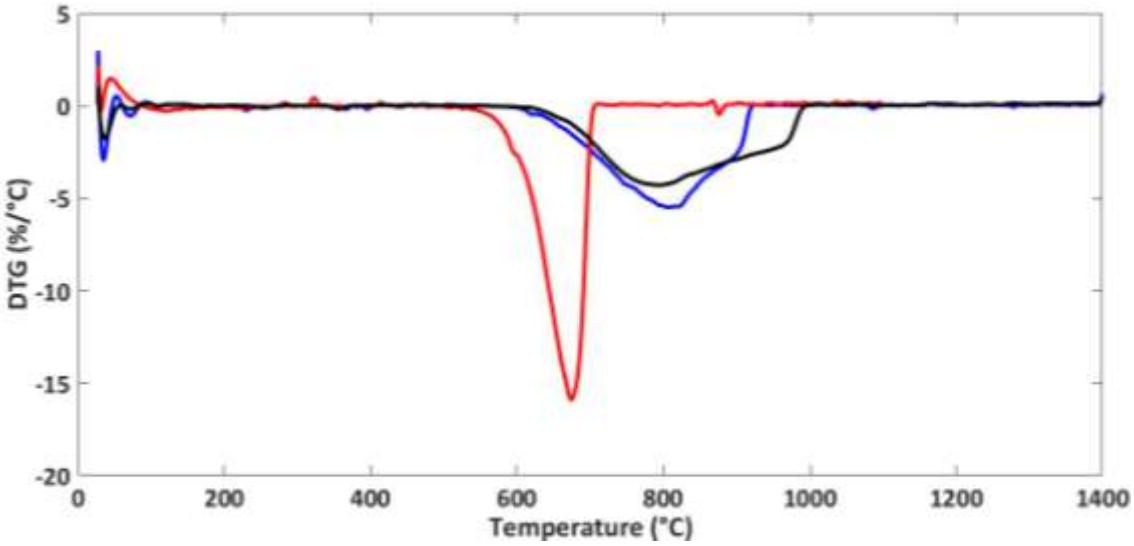

Figure 4.2. DTG curves of CNTs grown on different catalyst systems

As shown in Figure 4.2, sputter catalyst system has the narrowest DTG curve that means quality of CNTs grown on this catalyst are close to each other. On the other hand, reference and oxide-free catalyst systems have similar minimum point of rate at highest temperature point compared to others. So we can conclude that oxide-free and reference systems are usable respect to TGA results.

4.1.2 RAMAN Spectroscopy Results

To achieve the potential of CNTs, synthesis must have a high yield. Graphitization level is one of the most convenient and direct indication of yield and quality of CNT. Hence, RAMAN spectroscopy is a very useful and impactful technique to analyze

graphitization level; since, intensity of graphitized and amorphous carbon in excited area can be defined. Peak of graphitized carbon (G-peak) appears around 1580 cm^{-1} and peak of amorphous carbon or defect for our material (D-peak) appears around 1320 cm^{-1} of wavenumber. Positions of these peaks are depended on the wavelength of laser source. In our measurements, laser with 532 nm wavelength is used.

Intensities of G and D peaks represent the amount of graphitized and amorphous carbon in excited area by laser beam. Therefore, ratio between intensity of G-peak (I_G) and intensity of D-peak (I_D) gives the graphitization level of excited area.

To obtain the accurate graphitization level of a VA-CNT forest, RAMAN measurements must be taken from multiple points on VA-CNT forest, and must be repeated on at least three samples since distribution of CNT quality along the forest is inhomogeneous because of the nature of deposition techniques.

In this study, RAMAN measurements have been done on three different samples and five points each; in total, 15 measurements have been taken for every catalyst system presented, and every single sample has been growth under same conditions. RAMAN measurements that are closest to average have been used for comparison.

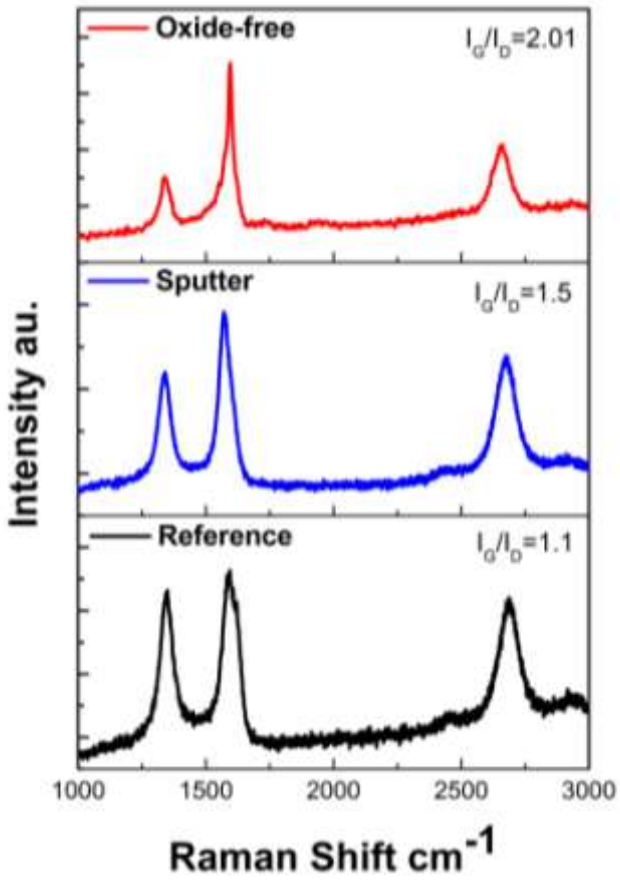

Figure 4.3. RAMAN shifts of reference, sputter and oxide-free catalyst system

As shown in Figure 4.3, intensity ratio of G and D peaks (I_G/I_D) for reference, sputter and oxide-free catalyst systems are 1.1, 1.5 and 2.01 respectively. Correspondingly, graphitization level of VA-CNT forests that are synthesized on reference catalyst system is the lowest one; according to that, lowest forest density is expected in this catalyst structure as discussed in further chapters. In order to obtain highest benefit from CNTs to carry load in nanocomposite, choosing VA-CNT forests with higher densities and graphitization levels as load carriers is more reasonable.

VA-CNT forests synthesized on sputter catalyst systems did not show significantly good results compared to oxide-free catalyst system. However, doing such comparison could have been wrong since thickness of iron layer of sputter catalyst system is not equal to other catalyst systems' iron layer thickness. As mentioned in previous chapters, sputter catalyst system has iron layer of 5 nm whereas other catalyst systems have 2 nm of it. This difference may have led benefit or loss on RAMAN result of samples. Since

the amount of iron in system is greater than others and the growth process is same (amount of carbon fed to system is constant) for all systems, extra iron might have adsorbed in its structure and decreased the intensity of G peak or might have healed the amorphous carbon that can stop the growth of CNT and increased the G peak. Due to this inequality, sputter system was not compared to other catalyst systems with respect to RAMAN results.

According to RAMAN results of reference and oxide-free catalyst systems, CNTs grown on oxide-free catalyst system is a better candidate for carrying load in nanocomposite since CNT density in excited volume is higher than reference, which means expected inter-tubular distance in VA-CNT forest grown on oxide-free catalyst structure is less than forest grown on reference catalyst system.

4.1.3 Comparison of Morphology

SEM images of VA-CNTs on different catalyst systems have been analyzed to better understand what is changing on morphology. In order to do that, images of VA-CNT forests have been used with 50kX and 200kX magnification, then compared. The main goal of this work is estimating how forest densities and waviness of CNTs are changed by changing catalyst structure.

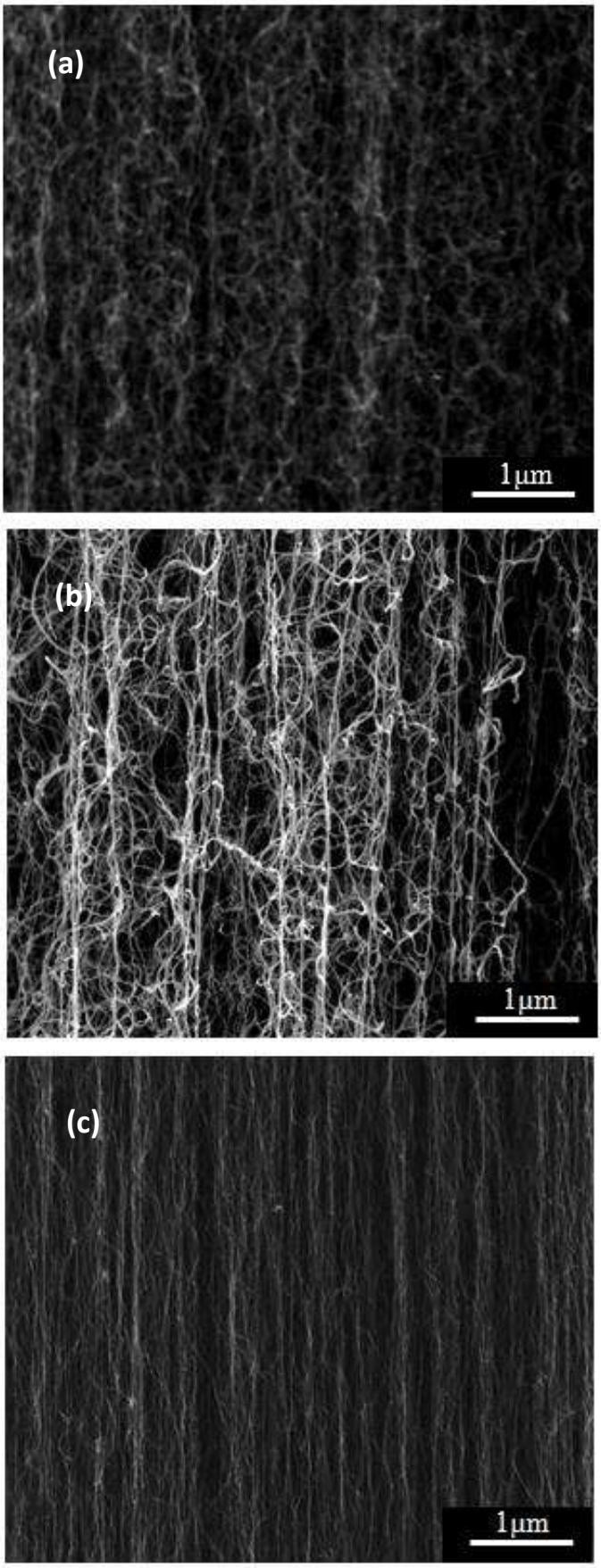

Figure 4.4. SEM images with 50k X magnification of VA-CNTs on a) reference b) sputter and c) oxide-free catalyst systems

As shown in Figure 4.4, inter-tubular distance is the smallest on oxide-free catalyst system. In other words, density of VA-CNT forest is the highest on this substrate, which also supports the RAMAN results. As seen in images, reference catalyst system has the lowest and sputter catalyst system has medial forest density whereas I_G/I_D is lowest for reference and highest for oxide-free catalyst system. This improvement on density is important to fabricate nanocomposites with higher volume fracture.

One other thing that might be discussed on these images is the waviness of CNTs. In 50k magnification images, it seems like CNTs become straight while density is increasing. However, SEM images with higher magnifications show that CNTs in high density forests are also in relatively wave form; that means, increasing density also increases the frequency of CNT waves.

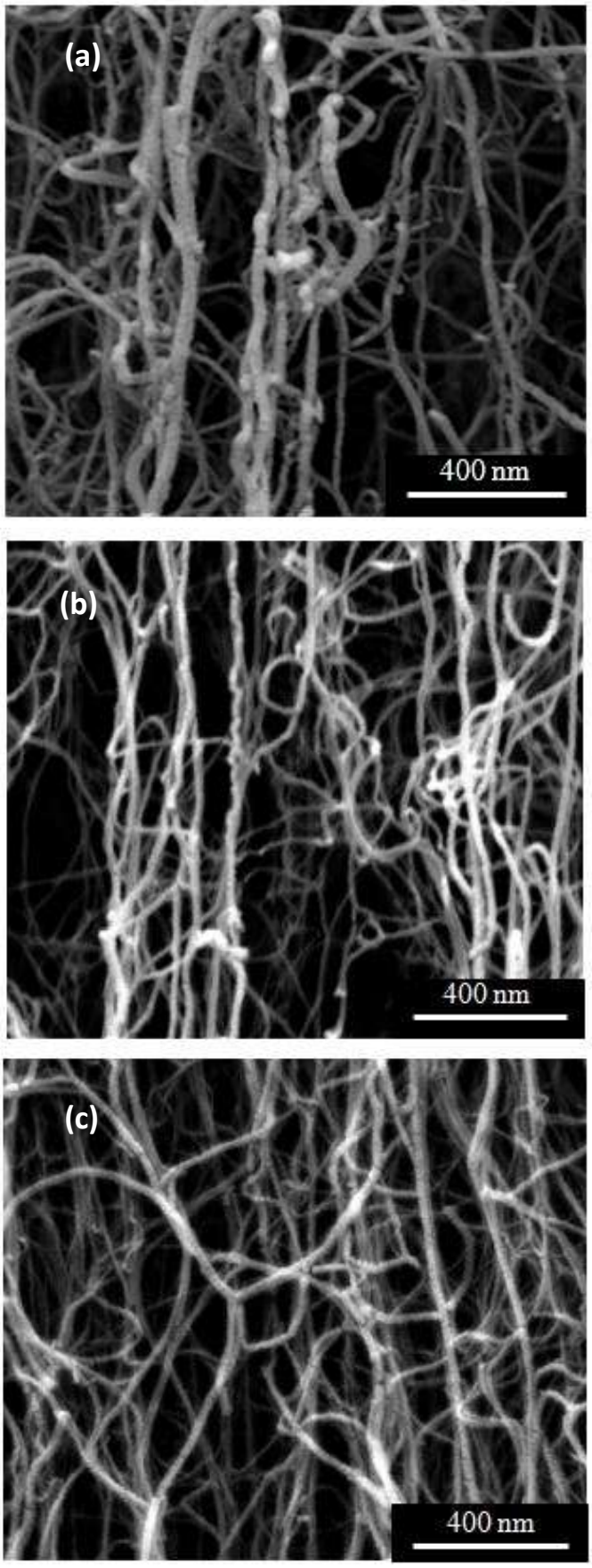

Figure 4.5. SEM images with 200k X magnification of VA-CNTs on a) reference b) sputter and c) oxide-free catalyst systems

Images shown in Figure 4.5 have been taken after CNTs are coated with gold. All samples are coated in one run, so it can be said that gold layers on CNTs are approximately equal. Hence, tube diameter of CNTs on different substrates can be compared. According to images, CNTs on reference catalyst system has the highest tube diameter and sputter has the smallest one. In addition, function parts are less frequent in SEM image of CNTs grown on oxide-free catalyst system which can be commented it cause decrease on waviness of CNTs.

To conclude, choosing VA-CNTs grown on oxide-free catalyst system may provide higher fiber volume fraction and load carry in unit fiber volume due to their high density, high waviness and relatively low tube diameter.

4.2 Effects of Substrate Roughness on Carbon Nanotube Morphology

In previous parts, it has been shown that by removing the silicon dioxide layer from catalyst system, graphitization level, correspondingly quality of CNTs has been improved. In this part, parameters that might be the reason behind that improvement of CNT quality by changing substrate systems are discussed. To do this investigation, similar catalyst systems are used. In addition to reference and oxide-free catalyst systems, a new system has been used to understand parameters. This new system has been fabricated on commercial <100> oriented silicon wafer with 300 nm thermal oxide layer. On the oxide layer, alumina and iron layers are coated by e-beam evaporator respectively like other catalyst systems. This catalyst system will be referred as thermal in future parts.

As mentioned in previous parts, silicon dioxide layer has a positive effect on CNT quality, since this layer avoids silicide formation; however, RAMAN results are not supporting this theory. To understand the reason behind those RAMAN results of reference, oxide-free and thermal catalyst systems have been compared. Samples that are used in comparison have been synthesized together to avoid any other factor that may affect the results.

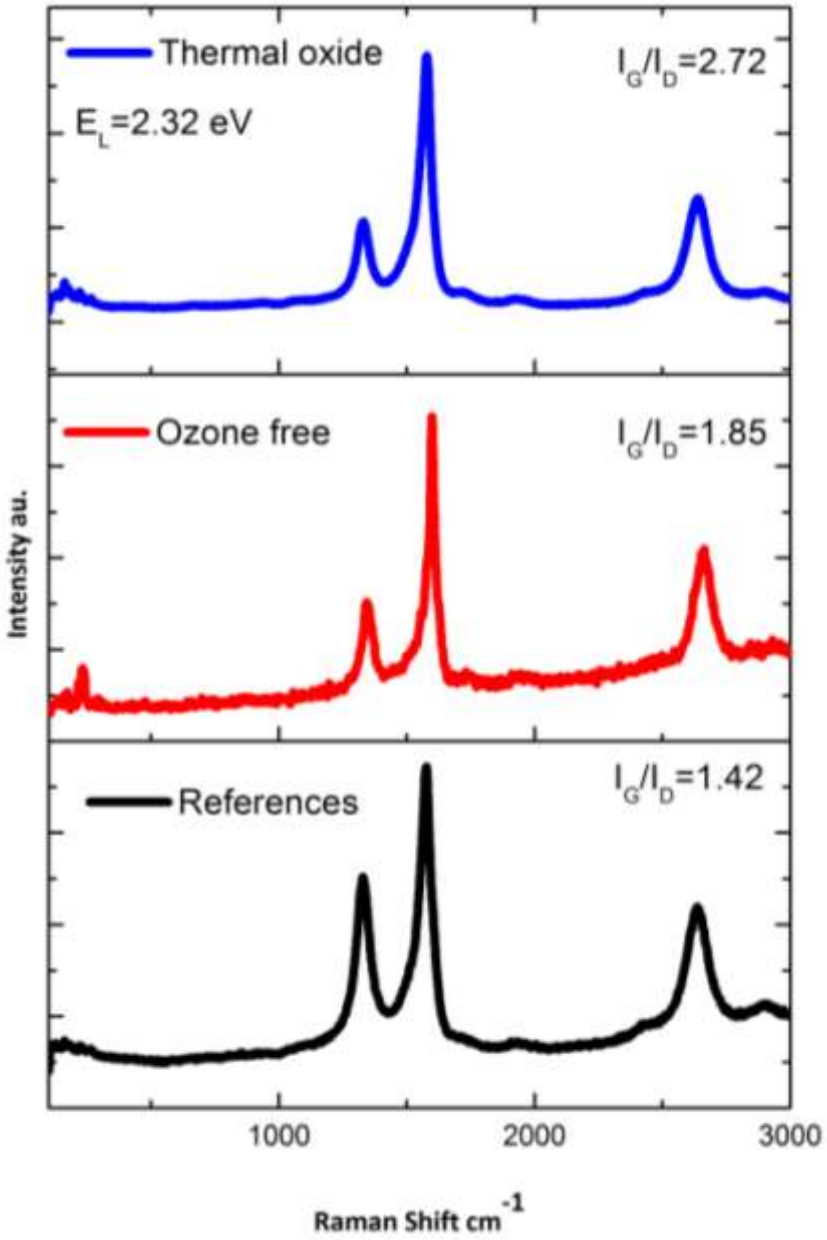

Figure 4.6. RAMAN shifts of reference, oxide-free and thermal oxide

As shown in Figure 4.6, thermal catalyst system gives the highest graphitization level even it involves silicon dioxide layer. Due to that, it has been understood that the problem is not the silicon oxide layer, it is the production method of this layer. Therefore, reference and thermal catalyst structures without alumina and iron layers are investigated deeply to understand what is different between these two substrates.

4.2.1 Roughness Measurements

The main difference between silicon dioxide layer of reference and thermal catalyst systems is the surface roughness of substrates. Since, thermal catalyst system has been applied on commercially available silicon wafer with oxide layer, substrate surface has been polished before applying alumina and iron layers unlike reference catalyst system. To show the affect of roughness on CNT quality, surface roughness of these substrates are measured with atomic force microscopy (AFM) and various angle spectroscopic ellipsometer (VASE).

Figure 4.7. Atomic Force Microscope used in roughness measurements

Figure 4.8. Various Angle Spectroscopic Ellipsometer

Surface roughness of reference catalyst system has been measured 4 nm by AFM and 8.8 nm by VASE. Surface roughness of thermal catalyst system on the other hand has been measured 0.5 nm by AFM and 2.7 by VASE. Even the measurement methods give different results; both measurement techniques show that surface roughness of reference catalyst system is higher than thermal catalyst system as expected. According to these results, it is concluded that roughness has a negative effect on CNT quality.

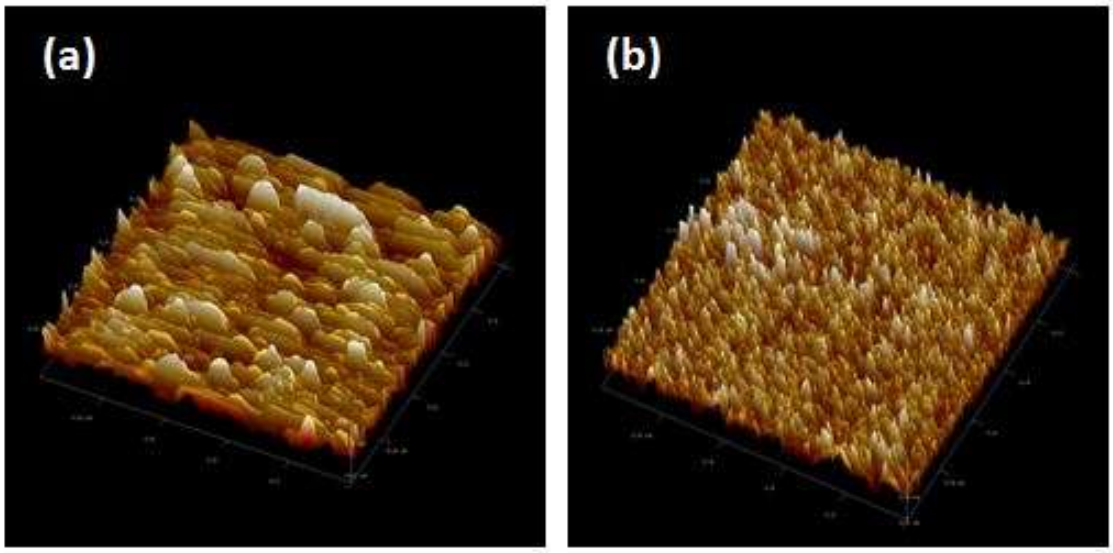

Figure 4.9. AFM histogram of (a) reference and (b) thermal catalyst systems

In order to understand the effect of roughness in detail, silicon dioxide layers with various surface roughness values have been produced. In this purpose, PE-CVD has been employed since it can generate surface roughness while coating silicon dioxide layer. To generate various surface roughness values, bare silicon wafers are coated silicon dioxide by PE-CVD with 75 nm/min constant coating rate up to four minutes. To do accurate thickness and surface roughness measurements, VASE has been employed instead of AFM; since tip of AFM is 50 nm sharp which is not precise for our experiments [93]. Surface roughness and silicon dioxide thickness change with respect to PE-CVD process time is shown in Figure 4.10.

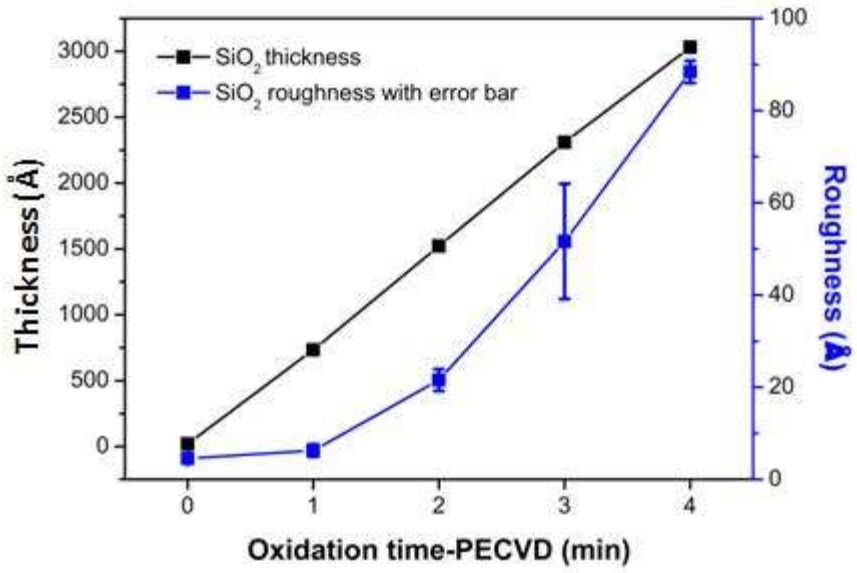

Figure 4.10. Surface roughness and SiO_2 thickness change by PE-CVD process time

As shown in results, surface roughness increases exponentially while oxide thickness increases linearly.

4.2.2 Roughness and Quality Relations

In this study, catalyst systems with various SiO_2 thicknesses and thermal catalyst system have been used in order to compare various surface roughness. Since the SiO_2 layer has a positive impact on CNT quality, various SiO_2 thickness and surface roughness must be optimized to achieve the highest graphitization level. In this work, thermal catalyst system will be the reference. The reason to choose thermal catalyst system as reference to this work is that system has both relatively smooth surface and high SiO_2 thickness. According to roughness measurements, substrate with 2 minutes oxidation process must have the highest graphitization level compared to other substrates since surface roughness value of that substrate is the closest one to thermal catalyst system. RAMAN results of substrate with various oxide thickness and thermal catalyst system is shown in Figure 4.11, and average I_G/I_D values by oxidization time is shown in Figure 4.12.

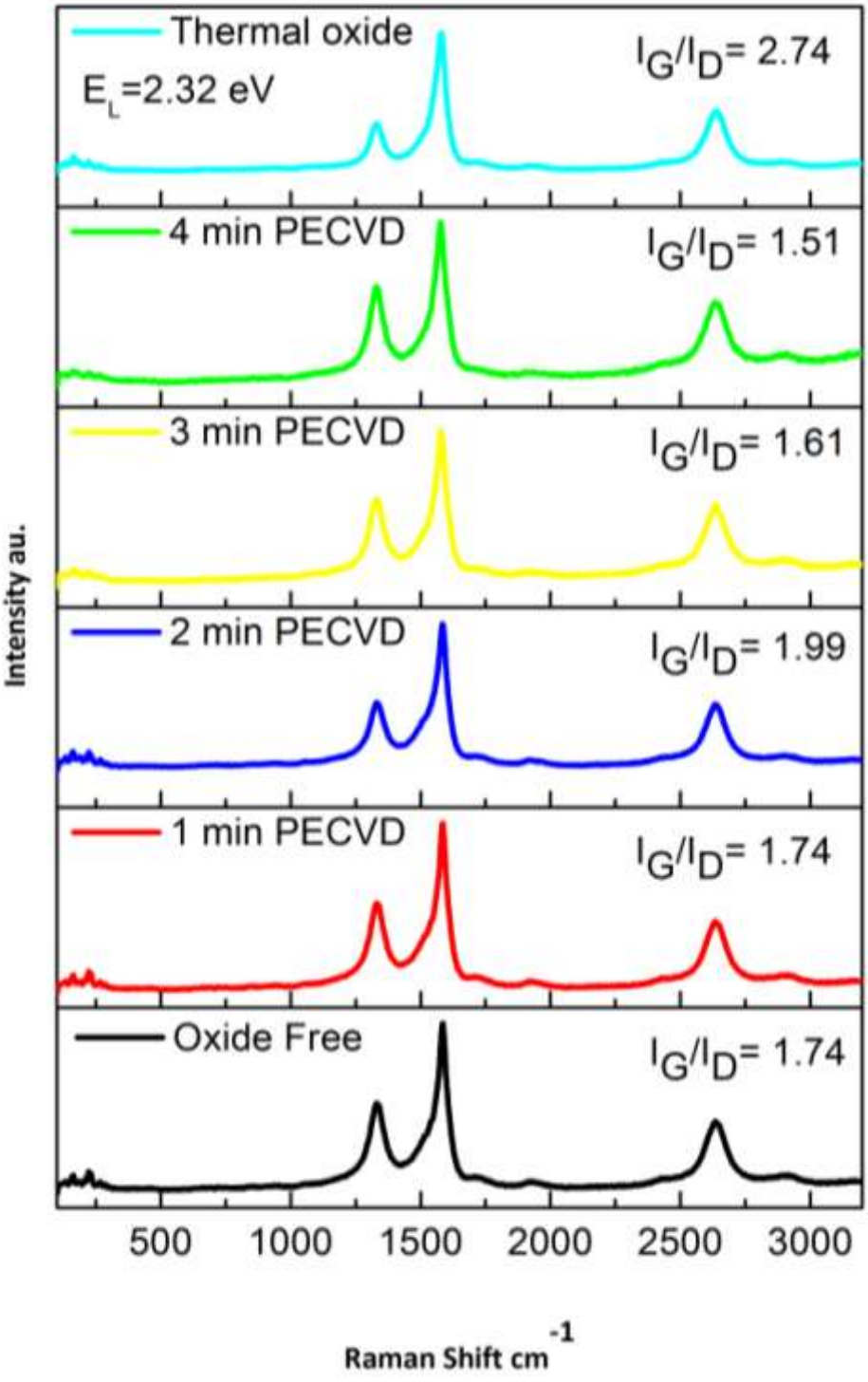

Figure 4.11. RAMAN results of various oxide thickness and thermal catalyst system

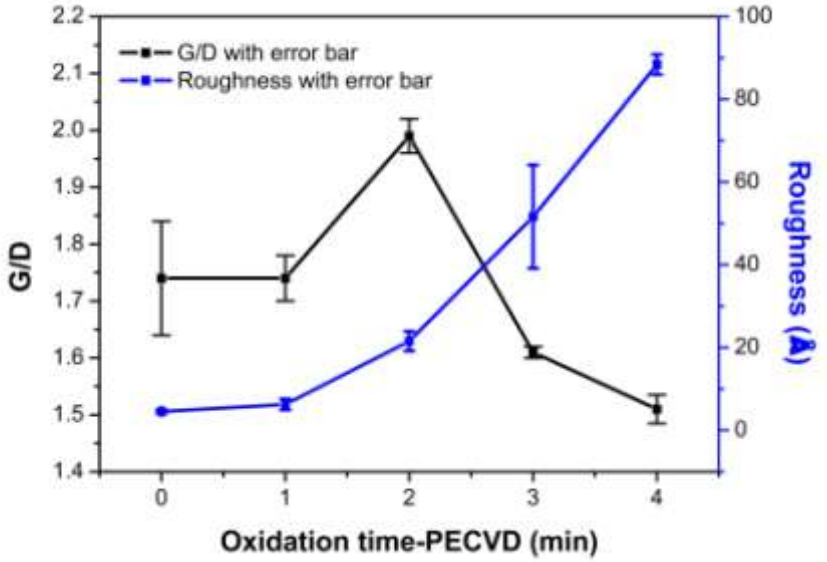

Figure 4.12. Change on ratio of intensities of G and D peaks by roughness

Every samples used in study are prepared and produced under same conditions to avoid other factors that may affect the results. Quarter of every sample are put in e-beam evaporator and coated in same run, then 1 cm by 1 cm pieces are cut from each substrate and growth in a single CCVD run, and every measurement is repeated 15 times from 3 different runs.

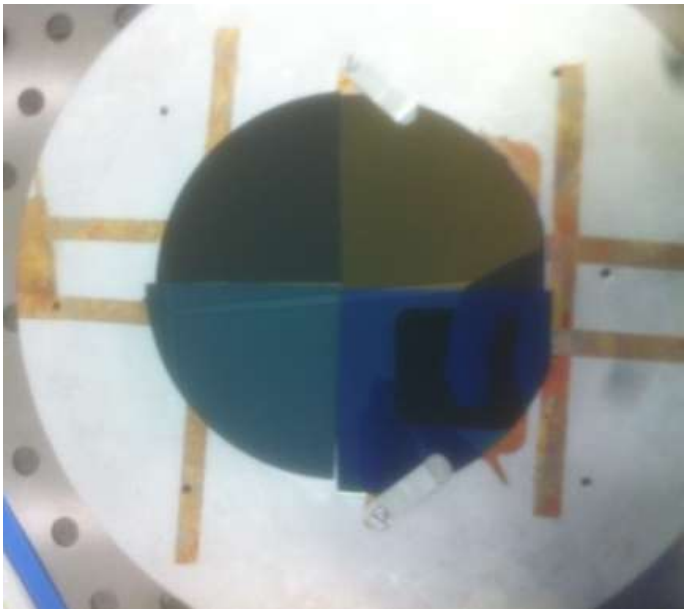

Figure 4.13. Quarter of substrates with various oxide thicknesses on same e-beam evaporator holder

The reason of improvement on quality of CNTs by optimizing surface roughness/SiO_2 thickness is increasing the probability of adsorption of free carbon by catalyst particles on substrate, since geometric interaction is one of the parameters affects adsorption.

4.3 Influence of Composite Preparation Methods on Mechanical Properties

In this part, mechanical behavior of neat epoxy, ozone treated oriented CNT-epoxy nanocomposite and treatment free oriented CNT-epoxy nanocomposites are compared. All of these nanocomposites are prepared by vacuum infusion method.

The main aim of this work is achieving highest mechanical properties by treating VA-CNT forests. In order to do that, various ozone treatment times are tried to obtain best results.

First of all, how CNT morphology is affected by ozone treatment is investigated. For this purpose, VA-CNT forests are treated up to 2 minutes with ozone then these samples and untreated sample are compared with respect to contact angle and RAMAN measurements.

Contact angle measurements have been performed with water on 5 samples from 0 second treated to 120 seconds treated first. Contact angle measurement results are shown in Table 4.1.

Table 4.1. Contact angle measurements with water

Treatment Time (s)	Contact Angle
0	130°
30	54°
60	-
90	-
120	-

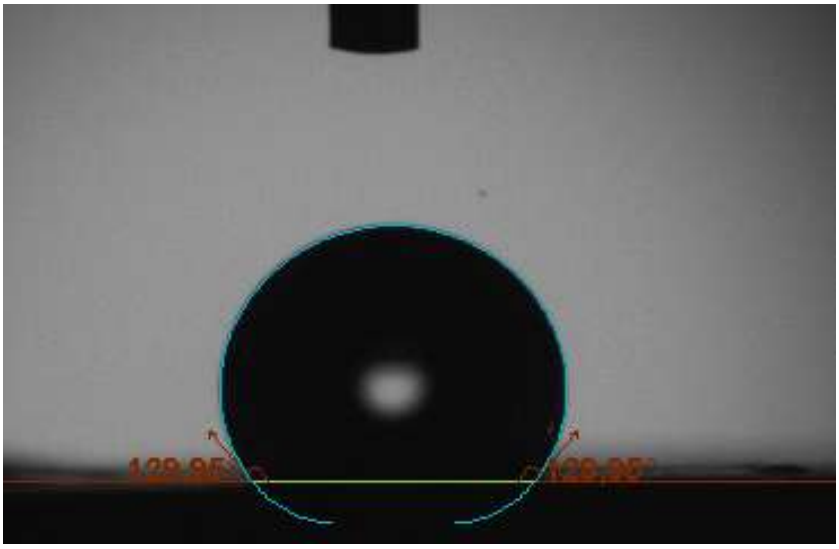

Figure 4.14. Contact angle measurement of untreated VA-CNT forest with water

As shown in Table 4.1, untreated VA-CNT forest shows a hydrophobic profile; although, with increasing ozone treatment time forest has become more hydrophilic and after one minute of treatment forest shows super-hydrophilic properties which is a sign of improvement on wettability. However, viscosity of water which is around 8.9×10^{-4} Pa.s at room temperature is much lower than epoxy used in nanocomposite. Due to that, this measurement has been repeated with epoxy which has a closer viscosity value to epoxy that has been used in nanocomposite fabrication. For this measurement, Momentive MGS L160 two component epoxy has been used since its viscosity is 0.7 Pa.s whereas viscosity of epoxy sheet is 0.6 Pa.s at 25 °C. Results of contact angle measurement with epoxy drop is shown in Table 4.2.

Table 4.2. Contact angle measurement with epoxy drop

Treatment Time (s)	Contact Angle
0	148°
30	112°
60	90°
90	88°
120	75°

Using epoxy for contact angle measurement increased the angle as expected; although, angle has kept decreasing with increasing treatment time same as water drop test. It can

be concluded that increasing ozone treatment has a positive impact on wettability of CNTs as long as it is applied. However, contact angle measurements are not enough to claim that ozone treatment is beneficial to improve mechanical properties of nanocomposite. RAMAN measurements of various ozone treated CNTs show that increasing ozone treatment time increases the D-peak; in other words, amount of defects or other organic groups in excited area are getting increase by increasing ozone treatment time. RAMAN peaks of various ozone treated CNTs are shown in Figure 4.15.

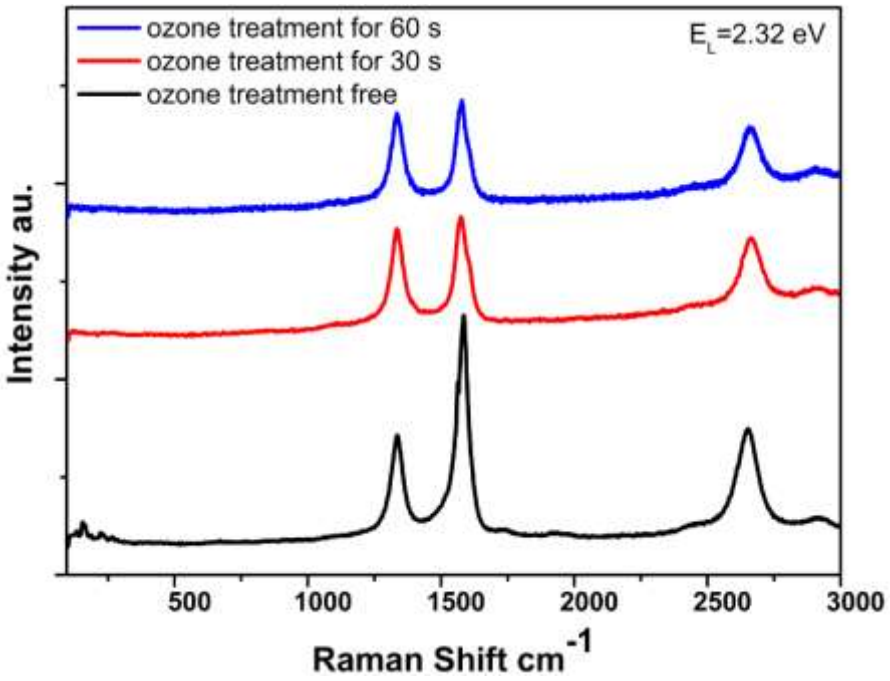

Figure 4.15. RAMAN shifts of various ozone treated CNTs

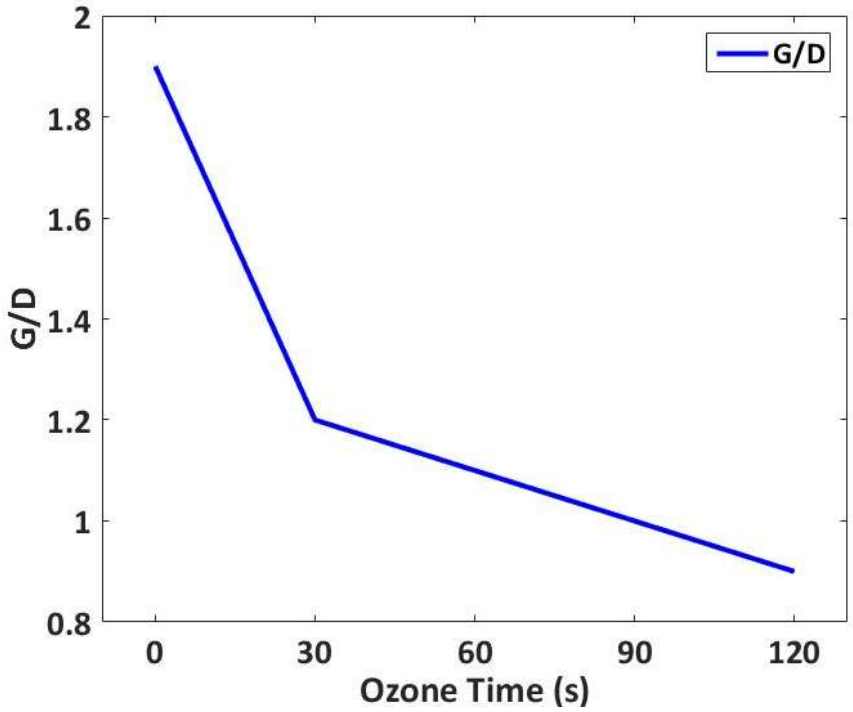

Figure 4.16. Change in ratio of G and D peaks by ozone treatment time

As shown in Figure 4.16, ozone treatment rapidly decreases the ratio of intensities of G and D peaks which means defects or other organic groups have been formed on VA-CNT forest by ozone treatments. In order to understand what is decreasing the G/D ratio, Fourier Transform Infrared Spectroscopy (FTIR) measurement has performed on VA-CNT forests before and after ozone treatment.

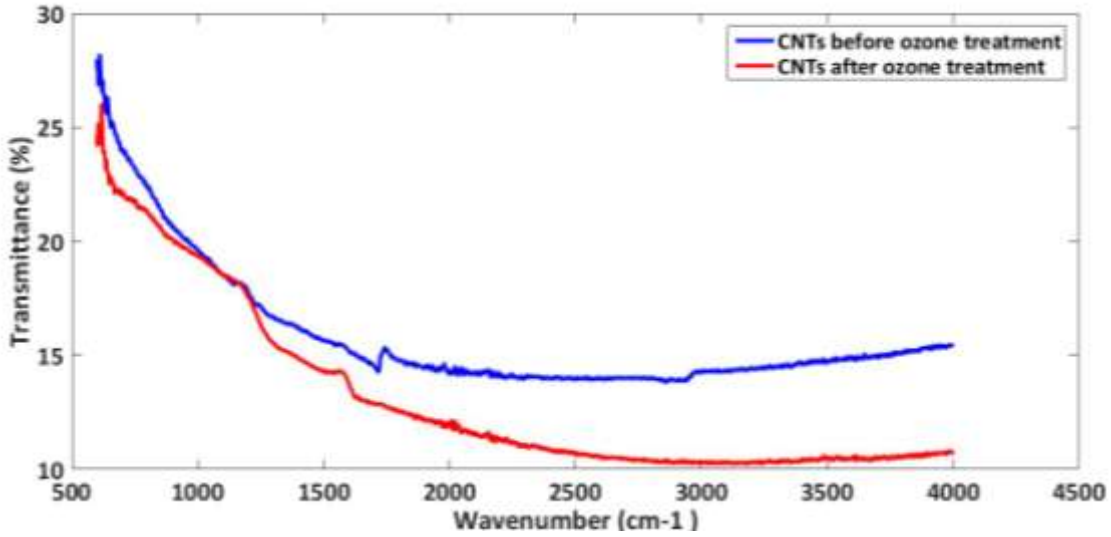

Figure 4.17. FTIR results of ozone treated VA-CNT forest

As shown in Figure 4.17, any peaks are observed on neither CNTs without treatment or CNTs after ozone treatment. Therefore, we can conclude that ozone treatment that we applied on VA-CNT forests does not form any other chemical groups; moreover, it can be said that this treatment most likely cause defects on VA-CNT forests.

Although, according to contact angle, RAMAN and FTIR results there is no way to say that ozone treatment is beneficial to mechanical properties of PNCs, and further mechanical tests are necessary to understand the influence of ozone treatment and in wake of these tests, ozone treatment time must be optimized.

4.3.1 Effect of Carbon Nanotube Reinforcement on Mechanical Properties

To distinguish the impact of ozone treatment, enhancement in mechanical properties by adding CNTs without ozone treatment must be shown. In order to do that, neat epoxy and CNT/epoxy nanocomposite are prepared and mechanical properties of these samples have been compared on DMA. Sample dimensions (33x8x1 mm) have been chosen according standard of tension film mode of DMA.

In addition to that, volume fraction of CNTs is needed to evaluate improvement on mechanical properties.

$$V_f = 1 - \frac{(1 - m_f)\rho_c}{\rho_m} \tag{4.1}$$

To calculate this fraction, equation (4.1) has been used; where V_f is volume fraction, m_f is mass of CNTs in nanocomposite, ρ_c is density of composite and ρ_m is density of matrix material.

Density of matrix material is known from data sheet of material and density of composite is calculated by dividing mass and volume of composite. To find only unknown of equation, m_f, TGA has been employed. To obtain the mass of CNTs in structure, a piece of nanocomposite is burned down under nitrogen atmosphere and the mass has been calculated by using the mass loss. Since CNTs do not breakdown under nitrogen atmosphere, remaining must be CNTs.

Density of composite (ρ_c) is calculated with,

$$\rho_c = \frac{m_c}{V_c} \tag{4.2}$$

Where m_c=0.1838 g and V_c=0.2304,

ρ_c=0.7977 g/cm^3

And ρ_m=1.56 g/cm^3 is given.

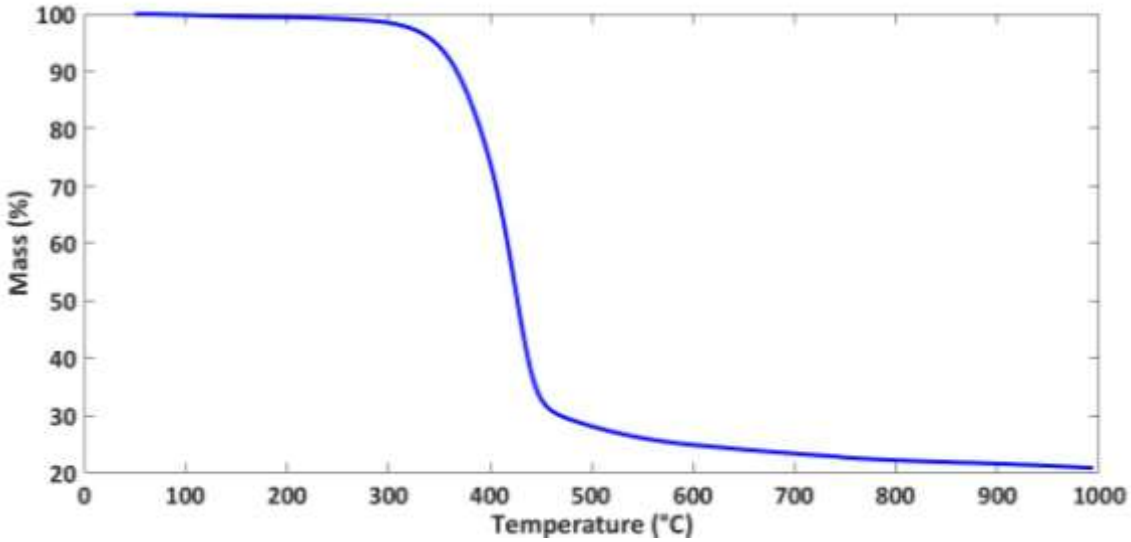

Figure 4.18. TGA curve of PNC under N_2 atmosphere

Mass fraction of CNTs (m_f) in PNCs is measured 21% with TGA. All values have been plugged to equation (4.2), and volume fraction of CNTs in PNCs has been calculated as 47%.

Before applying mechanical tests on samples, SEM images have been taken to ensure orientation of CNTs in PNCs. To take SEM images without changing the orientation of CNTs, PNC is frozen with liquid nitrogen then had been broken. As shown in Figure 4.19 and Figure 4.20, knock-down process provided the desired orientation.

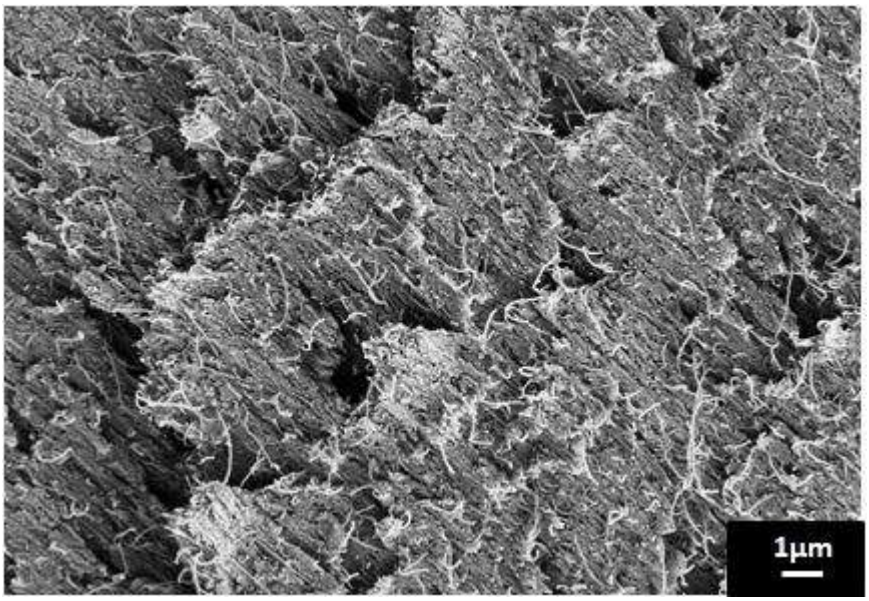

Figure 4.19. Top view of cross section of oriented PNC

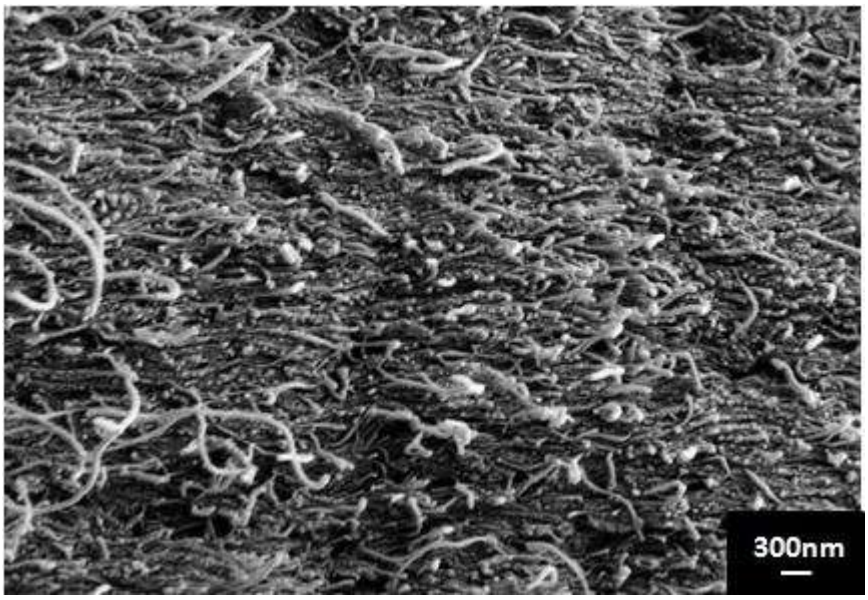

Figure 4.20. Side view of cross section of PNC

To observe impact of oriented CNT reinforcement on mechanical properties of PNCs, DMA tests had been applied on neat epoxy, prepared in dimensions of DMA standard, and oriented CNT reinforced PNC. Both static and dynamical measurements had been done and investigated.

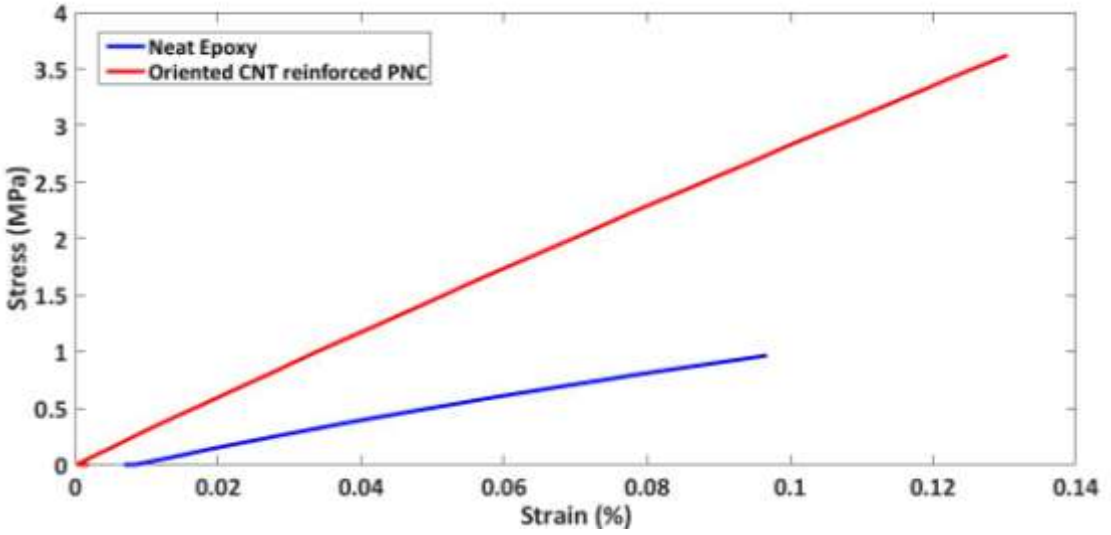

Figure 4.21. Static tension test on neat epoxy (blue) and oriented CNT reinforced PNC (red)

Young's modulus of oriented CNT reinforced PNC had been measured 2776 MPa whereas Young's modulus of neat epoxy had been measured 1093 MPa on tension tests (see Figure 4.21). According to these results, modulus has been improved 153.98% by oriented CNT reinforcement.

Beside of these results, multi-frequency dynamical tests had been done on same samples to observe how reinforcement affects the interval of working frequency.

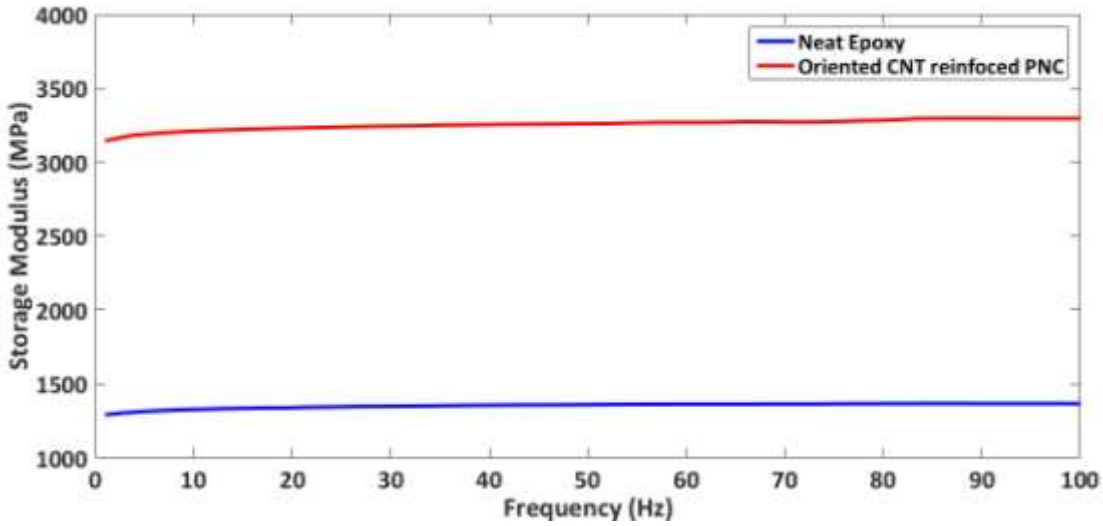

Figure 4.22. Storage modulus of neat epoxy (blue) and oriented CNT reinforced PNC (red) respect to frequency

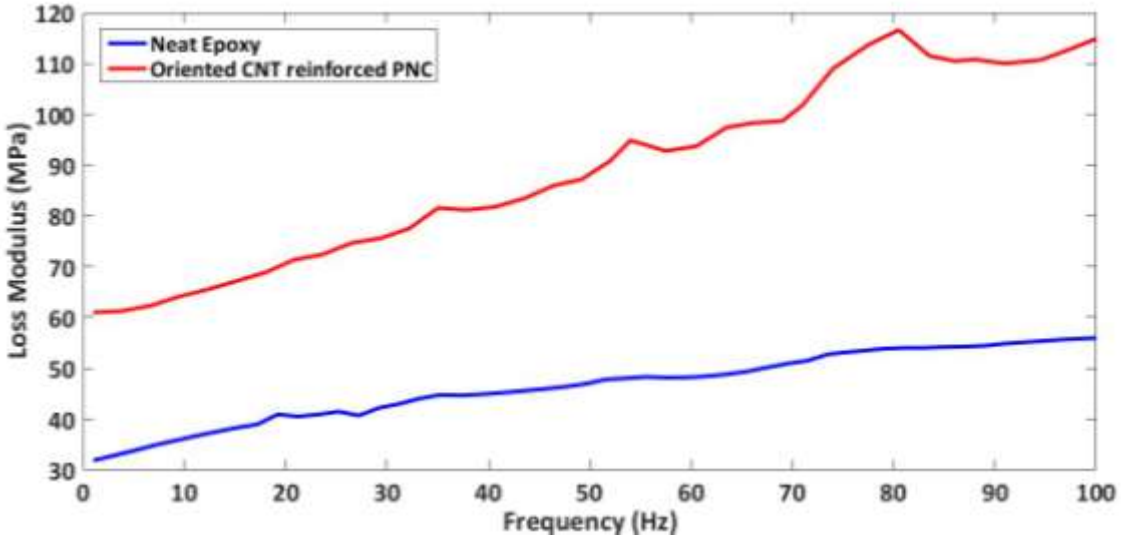

Figure 4.23. Loss modulus of neat epoxy (blue) and oriented CNT reinforced PNC (red) respect to frequency

As a result (shown in Figure 4.22 and Figure 4.23), storage modulus of neat epoxy had been measured 1325 MPa averagely whereas storage modulus of oriented CNT reinforced PNC had been 3300 MPa. According to that, it can be said that 149.06% improvement on storage modulus had been achieved by reinforcement. On the loss modulus part, neat epoxy had been measured 45MPa and PNC had been measured 80 MPa averagely. When viscoelastic properties of material is considered as summation of storage and loss modulus, it can be concluded that PNC shows elastic properties since only approximately 2.5% of total modulus is loss modulus independent from frequency. In addition, both storage and loss modulus increases by CNT reinforcement with correlation to static tension test.

4.3.2 Investigation of Ozone Treatment Process on Mechanical Properties

To observe the influence of ozone treatment on mechanical properties of PNCs, PNCs prepared with 30s ozone treated CNTs and ozone treatment free CNTs are prepared with same method and same orientation. Then, these samples are tested by DMA in single cantilever mode from 1 Hz to 100 Hz with maximum force of 12 N. The reason of choosing multi-frequency measurement is to observe the frequency interval that PNCs can work without any problems. This information is valuable for applications where durability on multi-frequency loads is important such as aerospace applications.

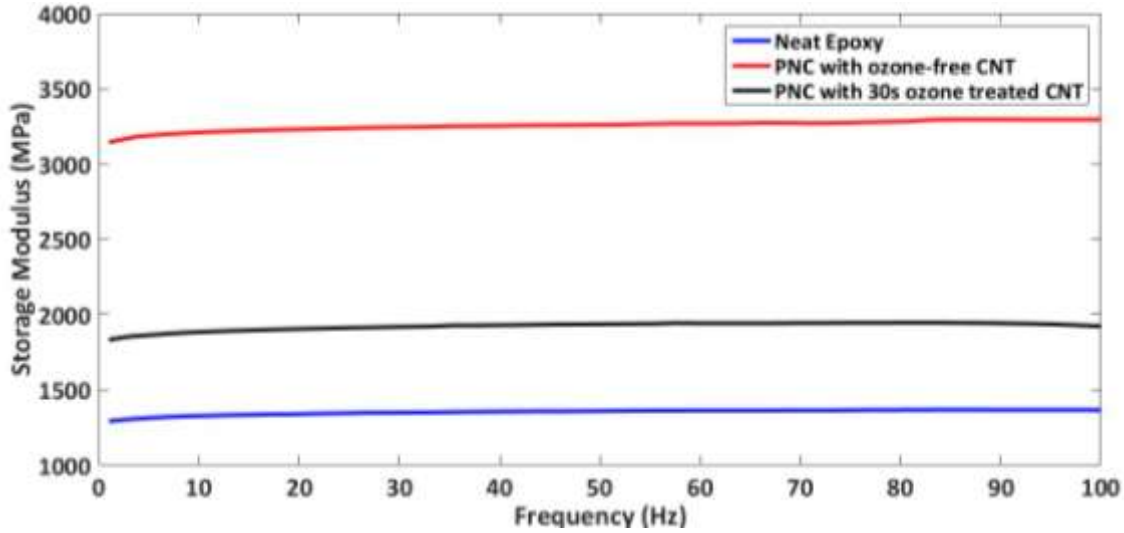

Figure 4.24. Storage modulus change of neat epoxy (blue), PNC with ozone treated CNTs (black) and PNC with ozone-free CNTs (red) respect to frequency

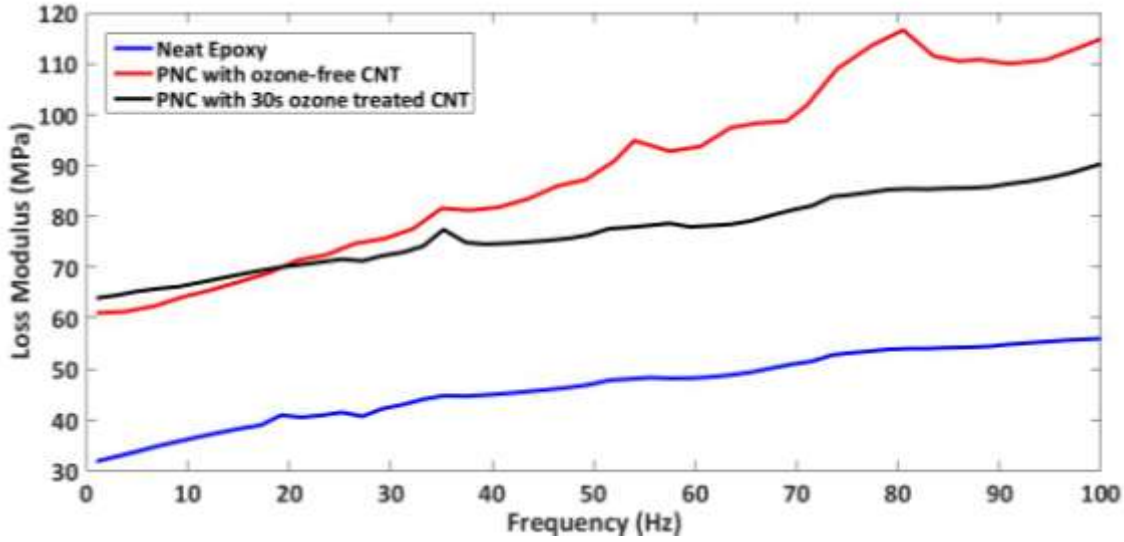

Figure 4.25. Loss modulus change of neat epoxy (blue), PNC with ozone treated CNTs (black) and PNC with ozone-free CNTs (red) respect to frequency

As shown in Figure 4.24, Figure 4.25, both of PNCs can work properly on all frequency range that applied. However, as a comparison, it can be said that loss modulus of both PNCs are similar whereas great difference on storage modulus. Storage modulus of PNC with 30s ozone treated has been measured 1950 MPa whereas storage modulus of PNC with ozone-free CNT is 3300 MPa. Therefore, it can be concluded that ozone treatment caused 69.23% of decrease on storage modulus independent form frequency. On the other hand, in loss modulus, it is shown that, difference between PNC with

ozone-free CNT and PNC with 30s ozone treated CNT is getting higher with increasing frequency. According to this change, it can be concluded that PNC with 30s ozone treated CNT is relatively less viscous in high frequencies.

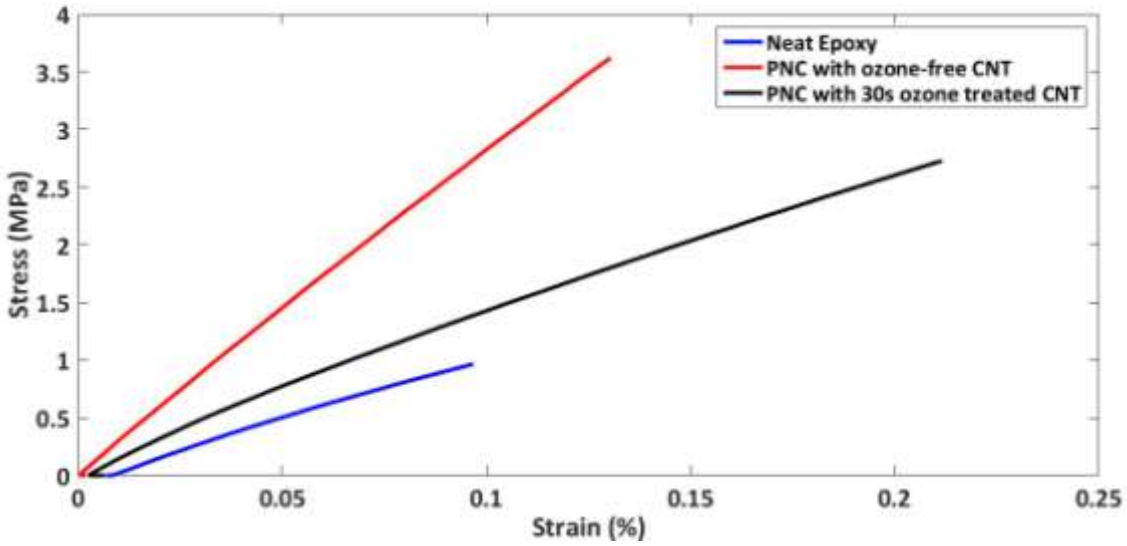

Figure 4.26. Static tension test of neat epoxy (blue), PNC with ozone treated CNTs (black) and PNC with ozone-free CNTs (red)

Young's modulus of PNC with 30s ozone treated CNTs had been measured 1409 MPa whereas young's modulus of PNC with ozone-free CNTs had been measured 2776 MPa which means 97.02% decrease on modulus. When static tension DMA results (see Figure 4.26) and change on RAMAN results by ozone treatment time (see Figure 4.16) are considered together, it can be concluded that ozone treatment mostly caused defects that reduce the mechanical properties of PNCs.

CHAPTER 5 Conclusion and Future Works

5.1 Conclusions

Main goal of this work was showing the influence of ozone treatment on mechanical behavior of oriented VA-CNT/Epoxy nanocomposites. On that road, many parameters that may enhance the mechanical properties of PNCs have been studied. Outcomes of these studies are,

1. How different catalyst structures can change the morphology of VA-CNTs has been studied and the best structure that serves to our aim has been developed.
2. Impact of substrate roughness on graphitization level of VA-CNTs has been discovered.
3. Changes on morphology of VA-CNTs after ozone treatment have been investigated, and relation between ozone treatment parameters and defect formation on VA-CNTs has been understood.
4. Oriented CNT/Epoxy nanocomposites with high volume fraction have been successfully fabricated.
5. Direct impact of ozone treatment on mechanical properties of PNCs has been studied.

5.2 Future Works

To improve the impact of study, there are five main work to do. First of all, sputter technique can be optimized to obtain same catalyst structure with other fabrication methods to do better comparison.

Secondly, in roughness study, instead of generating rough surfaces by coating various thicknesses of SiO_2, investigation of roughness can be done with constant oxide layer thickness; due to that, effect of oxide layer can be eliminated to show the effect of roughness clearly. Moreover, different carbon sources for CCVD process can be added to this work to understand the effect of adsorption mechanisms.

Finally, further mechanical tests can be done on PNCs produced with CNTs that are ozone treated with different parameter to understand relation between mechanical properties of PNCs and ozone treatment on CNTs. In addition, multi layers of CNTs oriented in various directions can be used to improve the mechanical properties of PNCs.

REFERENCES

[1] H. W. Kroto, J. R. Heath, S. C. O'Brien, R. F. Curl, and R. E. Smalley, "C 60: buckminsterfullerene," *Nature*, vol. 318, p. 162, 1985.

[2] S. Iijima, "Helical microtubules of graphitic carbon," *Nature*, vol. 354, pp. 56–58, 1991.

[3] R. Baughman, A. Zakhidov, and W. de Heer, "Carbon NanotubesOThe Route Toward Applications," *Science (80-.).*, vol. 297, no. 5582, pp. 787–792, 2002.

[4] M. S. Dresselhaus, G. Dresselhaus, and R. Saito, "Physics of carbon nanotubes," *Carbon N. Y.*, vol. 33, no. 7, pp. 883–891, 1995.

[5] E. T. Thostenson, Z. Ren, and T.-W. Chou, "Advances in the science and technology of carbon nanotubes and their composites: a review," *Compos. Sci. Technol.*, vol. 61, no. 13, pp. 1899–1912, 2001.

[6] M. S. Dresselhaus, G. Dresselhaus, and P. C. Eklund, "Chapter 20 – Applications of Carbon Nanostructures," in *Science of Fullerenes and Carbon Nanotubes*, 1996, pp. 870–917.

[7] B. I. Yakobson, C. J. Brabec, and J. Bernholc, "Nanomechanics of carbon tubes: Instabilities beyond linear response," *Phys. Rev. Lett.*, vol. 76, no. 14, pp. 2511–2514, 1996.

[8] C. Journet, W. K. Maser, P. Bernier, and a Loiseau, "Large-scale production of single-walled carbon nanotubes by the electric-arc technique," *Nature*, vol. 388, no. August, pp. 20–22, 1997.

[9] a G. Rinzler, J. Liu, H. Dai, P. Nikolaev, C. B. Huffman, F. J. Rodríguez-Macías, P. J. Boul, a H. Lu, D. Heymann, D. T. Colbert, R. S. Lee, J. E. Fischer, a M. Rao, P. C. Eklund, and R. E. Smalley, "Large-scale purification of single-wall carbon nanotubes: process, product, and characterization," *Appl. Phys. A Mater. Sci. Process.*, vol. 67, no. 1, pp. 29–37, 1998.

[10] P. Nikolaev, M. J. Bronikowski, R. K. Bradley, F. Rohmund, D. T. Colbert, K. a Smith, and R. E. Smalley, "Gas-phase catalytic growth of single-walled carbon nanotubes from carbon monoxide," *Chem. Phys. Lett.*, vol. 313, no. 1–2, pp. 91–97, 1999.

[11] Z. F. Ren, Z. P. Huang, D. Z. Wang, J. G. Wen, J. W. Xu, J. H. Wang, L. E. Calvet, J. Chen, J. F. Klemic, and M. a Reed, "Growth of a single freestanding multiwall carbon nanotube on each nanonickel dot," *Appl. Phys. Lett.*, vol. 75, no. 8, pp. 1086–1088, 1999.

[12] G. Overney, W. Zhong, and D. Tomanek, "Structural Rigidity and Low-Frequency Vibrational-Modes of Long Carbon Tubules," *Zeitschrift Fur Phys. D-Atoms Mol. Clust.*, vol. 27, no. 1, pp. 93–96, 1993.

[13] M. M. J. Treacy, T. W. Ebbesen, and J. M. Gibson, "Exceptionally high Young's modulus observed for individual carbon nanotubes," *Nature*, vol. 381, no. 6584, pp. 678–680, 1996.

[14] E. W. Wong, P. E. Sheehan, and C. M. Lieber, "Nanobeam Mechanics: Elasticity, Strength, and Toughness of Nanorods and Nanotubes," *Science (80-.).*, vol. 277, no. 5334, pp. 1971–1975, 1997.

[15] S. Iijima and T. Ichihashi, "Single-shell carbon nanotubes of 1-nm diameter," *Nature*, vol. 363, pp. 603–605, 1993.

[16] D. S. Bethune, C. H. Klang, M. S. de Vries, G. Gorman, R. Savoy, J. Vazquez, and R. Beyers, "Cobalt-catalysed growth of carbon nanotubes with single-atomic-layer walls," *Nature*, vol. 363, no. 6430, pp. 605–607, 1993.

[17] C.-L. Wu, H.-C. Lin, J.-S. Hsu, M.-C. Yip, and W. Fang, "Static and dynamic mechanical properties of polydimethylsiloxane/carbon nanotube nanocomposites," *Thin Solid Films*, vol. 517, no. 17, pp. 4895–4901, 2009.
[18] Z. Shi, Y. Lian, F. H. Liao, X. Zhou, Z. Gu, Y. Zhang, S. Iijima, H. Li, K. T. Yue, and S. L. Zhang, "Large scale synthesis of single-wall carbon nanotubes by arc-discharge method," *J. Phys. Chem. Solids*, vol. 61, no. 7, pp. 1031–1036, 2000.
[19] Y. Saito, K. Nishikubo, K. Kawabata, and T. Matsumoto, "Carbon nanocapsules and single-layered nanotubes produced with platinum-group metals (Ru, Rh, Pd, Os, Ir, Pt) by arc discharge," *J. Appl. Phys.*, vol. 80, no. 5, p. 3062, 1996.
[20] a. Thess, R. Lee, P. Nikolaev, H. Dai, P. Petit, J. Robert, C. Xu, Y. H. Lee, S. G. Kim, a. G. Rinzler, D. T. Colbert, G. E. Scuseria, D. Tomanek, J. E. Fischer, and R. E. Smalley, "Crystalline Ropes of Metallic Carbon Nanotubes," *Science (80-.).*, vol. 273, no. 5274, pp. 483–487, 1996.
[21] Y. Zhang and S. Iijima, "Formation of single-wall carbon nanotubes by laser ablation of fullerenes at low temperature," *Appl. Phys. Lett.*, vol. 75, no. 20, pp. 3087–3089, 1999.
[22] P. G. Collins and P. Avouris, "Nanotubes for electronics.," *Sci. Am.*, vol. 283, no. 6, pp. 62–69, 2000.
[23] M. Ge and K. Sattler, "Bundles of carbon nanotubes generated by vapor-phase growth," *Appl. Phys. Lett.*, vol. 64, no. 6, pp. 710–711, 1994.
[24] R. Seidel, G. S. Duesberg, E. Unger, a. P. Graham, M. Liebau, and F. Kreupl, "Chemical Vapor Deposition Growth of Single-Walled Carbon Nanotubes at 600 °C and a Simple Growth Model," *J. Phys. Chem. B*, vol. 108, no. 6, pp. 1888–1893, 2004.
[25] H. Dai, "Carbon nanotubes: Synthesis, integration, and properties," *Acc. Chem. Res.*, vol. 35, no. 12, pp. 1035–1044, 2002.
[26] W. Z. Li, S. S. Xie, L. X. Qian, B. H. Chang, B. S. Zou, W. Y. Zhou, R. A. Zhao, and G. Wang, "Large-Scale Synthesis of Aligned Carbon Nanotubes," *Nature*, vol. 274, no. December, pp. 1701–1703, 1996.
[27] H. Cebeci, "MULTIFUNCTIONAL PROPERTIES OF CONTROLLED MORPHOLOGY ALIGNED CARBON NANOTUBE POLYMER NANOCOMPOSITES AND THEIR APPLICATIONS," 2011.
[28] C. N. R. Rao and R. Sen, "Large aligned-nanotube bundles from ferrocene pyrolysis," *Chem. Commun.*, no. 15, pp. 1525–1526, 1998.
[29] L. Dai, "Controlled growth and modification of aligned carbon nanotubes for multifunctional nanocomposites and nanodevices," in *INEC 2010 - 2010 3rd International Nanoelectronics Conference, Proceedings*, 2010, pp. 45–46.
[30] A. J. Hart and A. H. Slocum, "Rapid growth and flow-mediated nucleation of millimeter-scale aligned carbon nanotube structures from a thin-film catalyst," *J. Phys. Chem. B*, vol. 110, no. 16, pp. 8250–8257, 2006.
[31] S. B. Sinnott, R. Andrews, D. Qian, A. M. Rao, Z. Mao, E. C. Dickey, and F. Derbyshire, "Model of carbon nanotube growth through chemical vapor deposition," *Chem. Phys. Lett.*, vol. 315, no. 1–2, pp. 25–30, 1999.
[32] R. T. K. Baker, P. S. Harris, R. B. Thomas, and R. J. Waite, "Formation of filamentous carbon from iron, cobalt and chromium catalyzed decomposition of acetylene," *J. Catal.*, vol. 30, no. 1, pp. 86–95, 1973.
[33] F. Ding, K. Bolton, and A. Rosén, "Nucleation and Growth of Single-Walled Carbon Nanotubes: A Molecular Dynamics Study," *J. Phys. Chem. B*, vol. 108, no. 45, pp. 17369–17377, Nov. 2004.

[34] Y. Homma, Y. Kobayashi, T. Ogino, D. Takagi, R. Ito, Y. J. Y. Y. J. Jung, and P. M. P. Ajayan, “Role of Transition Metal Catalysts in Single-Walled Carbon Nanotube Growth in Chemical Vapor Deposition,” *J. Phys. Chem. B*, vol. 107, no. 44, pp. 12161–12164, 2003.
[35] Y. Y. Wei, G. Eres, V. I. Merkulov, and D. H. Lowndes, “Effect of catalyst film thickness on carbon nanotube growth by selective area chemical vapor deposition,” *Appl. Phys. Lett.*, vol. 78, no. 10, p. 1394, 2001.
[36] P. M. Ajayan, “Nanotubes from Carbon.,” *Chem. Rev.*, vol. 99, no. 7, pp. 1787–1800, 1999.
[37] J. N. Coleman, U. Khan, W. J. Blau, and Y. K. Gun’ko, “Small but strong: A review of the mechanical properties of carbon nanotube-polymer composites,” *Carbon N. Y.*, vol. 44, no. 9, pp. 1624–1652, 2006.
[38] Z. Spitalsky, D. Tasis, K. Papagelis, and C. Galiotis, “Carbon nanotube-polymer composites: Chemistry, processing, mechanical and electrical properties,” *Prog. Polym. Sci.*, vol. 35, no. 3, pp. 357–401, 2010.
[39] P. M. Ajayan, O. Stephan, C. Colliex, and D. Trauth, “Aligned Carbon Nanotube Arrays Formed by Cutting a Polymer Resin-Nanotube Composite.” 1994.
[40] P. C. Ma, N. A. Siddiqui, G. Marom, and J. K. Kim, “Dispersion and functionalization of carbon nanotubes for polymer-based nanocomposites: A review,” *Compos. Part A Appl. Sci. Manuf.*, vol. 41, no. 10, pp. 1345–1367, 2010.
[41] A. Allaoui, S. Bai, H. . Cheng, and J. . Bai, “Mechanical and electrical properties of a MWNT/epoxy composite,” *Compos. Sci. Technol.*, vol. 62, no. 15, pp. 1993–1998, 2002.
[42] A. T. Sepúlveda, R. Guzman de Villoria, J. C. Viana, A. J. Pontes, B. L. Wardle, and L. A. Rocha, “Full elastic constitutive relation of non-isotropic aligned-CNT/PDMS flexible nanocomposites,” *Nanoscale*, vol. 5, no. 11, p. 4847, 2013.
[43] A. V. Melechko, V. I. Merkulov, T. E. McKnight, M. A. Guillorn, K. L. Klein, D. H. Lowndes, and M. L. Simpson, “Vertically aligned carbon nanofibers and related structures: Controlled synthesis and directed assembly,” *J. Appl. Phys.*, vol. 97, no. 4, 2005.
[44] W. Ma, L. Liu, Z. Zhang, R. Yang, G. Liu, T. Zhang, X. An, X. Yi, Y. Ren, Z. Niu, J. Li, H. Dong, W. Zhou, P. M. Ajayan, and S. Xie, “High-strength composite fibers: realizing true potential of carbon nanotubes in polymer matrix through continuous reticulate architecture and molecular level couplings.,” *Nano Lett.*, vol. 9, no. 8, pp. 2855–61, Aug. 2009.
[45] B. L. Wardle, D. S. Saito, E. J. Garc??a, A. J. Hart, R. Guzm??n De Villoria, and E. A. Verploegen, “Fabrication and characterization of ultrahigh-volume-fraction aligned carbon nanotube-polymer composites,” *Adv. Mater.*, vol. 20, no. 14, pp. 2707–2714, 2008.
[46] M. Moniruzzaman and K. I. Winey, “Polymer nanocomposites containing carbon nanotubes,” *Macromolecules*, vol. 39, no. 16. pp. 5194–5205, 2006.
[47] P. Pötschke, A. R. Bhattacharyya, A. Janke, and H. Goering, “Melt mixing of polycarbonate/multi-wall carbon nanotube composites,” *Compos. Interfaces*, vol. 10, no. 4–5, pp. 389–404, 2003.
[48] I. Y. Phang, L. Shen, S. Y. Chow, and W.-D. Zhang, “Morphology and Mechanical Properties of Multiwalled Carbon Nanotubes Reinforced Nylon-6 Composites,” *Macromolecules*, vol. 37, no. 19, pp. 7214–7222, Sep. 2004.
[49] A. R. Bhattacharyya, T. . Sreekumar, T. Liu, S. Kumar, L. M. Ericson, R. H. Hauge, and R. E. Smalley, “Crystallization and orientation studies in

polypropylene/single wall carbon nanotube composite," *Polymer (Guildf).*, vol. 44, no. 8, pp. 2373–2377, 2003.
[50] E. J. Siochi, D. C. Working, C. Park, P. T. Lillehei, J. H. Rouse, C. C. Topping, A. R. Bhattacharyya, and S. Kumar, "Melt processing of SWCNT-polyimide nanocomposite fibers," *Compos. Part B Eng.*, vol. 35, no. 5, pp. 439–446, 2004.
[51] S. Barrau, P. Demont, E. Perez, A. Peigney, C. Laurent, and C. Lacabanne, "Effect of Palmitic Acid on the Electrical Conductivity of Carbon Nanotubes−Epoxy Resin Composites," *Macromolecules*, vol. 36, no. 26, pp. 9678–9680, Dec. 2003.
[52] K. S. Kim, Z. Lin, P. Shrotriya, S. Sundararajan, and Q. Zou, "Iterative control approach to high-speed force-distance curve measurement using AFM: Time-dependent response of PDMS example," *Ultramicroscopy*, vol. 108, no. 9, pp. 911–920, 2008.
[53] P. R. Sundararajan, S. Singh, and M. Moniruzzaman, "Surfactant-Induced Crystallization of Polycarbonate," *Macromolecules*, vol. 37, no. 26, pp. 10208–10211, Dec. 2004.
[54] J. Zhu, J. Kim, H. Peng, J. L. Margrave, V. N. Khabashesku, and E. V. Barrera, "Improving the Dispersion and Integration of Single-Walled Carbon Nanotubes in Epoxy Composites through Functionalization," *Nano Lett.*, vol. 3, no. 8, pp. 1107–1113, Aug. 2003.
[55] J. Zhu, H. Peng, F. Rodriguez-Macias, J. L. Margrave, V. N. Khabashesku, A. M. Imam, K. Lozano, and E. V. Barrera, "Reinforcing epoxy polymer composites through covalent integration of functionalized nanotubes," *Adv. Funct. Mater.*, vol. 14, no. 7, pp. 643–648, 2004.
[56] J. N. Coleman, U. Khan, and Y. K. Gun'ko, "Mechanical Reinforcement of Polymers Using Carbon Nanotubes," *Adv. Mater.*, vol. 18, no. 6, pp. 689–706, 2006.
[57] L. S. Schadler, S. C. Giannaris, and P. M. Ajayan, "Load transfer in carbon nanotube epoxy composites," *Appl. Phys. Lett.*, vol. 73, no. 26, p. 3842, 1998.
[58] M. Mecklenburg, D. Mizushima, N. Ohtake, W. Bauhofer, B. Fiedler, and K. Schulte, "On the manufacturing and electrical and mechanical properties of ultra-high wt.% fraction aligned MWCNT and randomly oriented CNT epoxy composites," *Carbon N. Y.*, vol. 91, pp. 275–290, 2015.
[59] P. D. Bradford, X. Wang, H. Zhao, J. P. Maria, Q. Jia, and Y. T. Zhu, "A novel approach to fabricate high volume fraction nanocomposites with long aligned carbon nanotubes," *Compos. Sci. Technol.*, vol. 70, no. 13, pp. 1980–1985, 2010.
[60] W. Callister and D. Rethwisch, *Materials science and engineering: an introduction*, vol. 94. 2007.
[61] H. L. Cox, "The elasticity and strength of paper and other fibrous materials," *Br. J. Appl. Phys.*, vol. 3, no. 3, pp. 72–79, 2002.
[62] G. P. Carman and K. L. Reifsnider, "Micromechanics of short-fiber composites," *Compos. Sci. Technol.*, vol. 43, no. 2, pp. 137–146, 1992.
[63] J. C. H. Affdl and J. L. Kardos, "The Halpin???Tsai equations: A review," *Polymer Engineering & Science*, vol. 16, no. 5. pp. 344–352, 1976.
[64] P. M. Ajayan, L. S. Schadler, C. Giannaris, and A. Rubio, "Single-walled carbon nanotube-polymer composites: Strength and weakness," *Adv. Mater.*, vol. 12, no. 10, pp. 750–753, 2000.
[65] M. A. L. Manchado, L. Valentini, J. Biagiotti, and J. M. Kenny, "Thermal and mechanical properties of single-walled carbon nanotubes-polypropylene composites prepared by melt processing," *Carbon N. Y.*, vol. 43, no. 7, pp. 1499–

1505, 2005.
[66] C. A. Cooper, R. J. Young, and M. Halsall, “Investigation into the deformation of carbon nanotubes and their composites through the use of Raman spectroscopy,” *Compos. Part A Appl. Sci. Manuf.*, vol. 32, no. 3–4, pp. 401–411, 2001.
[67] M. A. Azam, N. S. A. Manaf, E. Talib, and M. S. A. Bistamam, “Aligned carbon nanotube from catalytic chemical vapor deposition technique for energy storage device: a review,” *Ionics (Kiel).*, vol. 19, no. 11, pp. 1455–1476, 2013.
[68] Z. Yu, L. Tetard, L. Zhai, and J. Thomas, “Supercapacitor electrode materials: nanostructures from 0 to 3 dimensions,” *Energy Environ. Sci.*, vol. 8, no. 3, pp. 702–730, 2015.
[69] J. Sinclair, “An Introduction to Carbon Nanotubes,” *Carbon Nanotubes*. pp. 1–8, 2009.
[70] V. N. Popov, “Carbon nanotubes: Properties and application,” *Materials Science and Engineering R: Reports*, vol. 43, no. 3. pp. 61–102, 2004.
[71] and Z. A. B. C. Mohamed ShuaibMohamed Saheed, NoraniMutiMohamed, “Effect of Different Catalyst Deposition Technique on Aligned Multiwalled Carbon Nanotubes Grown by Thermal Chemical Vapor Deposition,” *J. Nanomater.*, vol. 2014, pp. 1–11, 2014.
[72] C. R. Oliver, E. S. Polsen, E. R. Meshot, S. Tawfick, S. J. Park, M. Bedewy, and A. J. Hart, “A Statistical Analysis of Variation in Laboratory Growth of Carbon Nanotube Forests and Recommendations for Improvement of Process Consistency.,” *ACS Nano*, vol. 7, no. 4, pp. 3565–3580, 2013.
[73] B. H. Choi, H. Yoo, Y. B. Kim, and J. H. Lee, “Effects of Al buffer layer on growth of highly vertically aligned carbon nanotube forests for in situ yarning,” *Microelectron. Eng.*, vol. 87, no. 5–8, pp. 1500–1505, 2010.
[74] H. Liu, Y. Zhang, D. Arato, R. Li, P. Mérel, and X. Sun, “Aligned multi-walled carbon nanotubes on different substrates by floating catalyst chemical vapor deposition: Critical effects of buffer layer,” *Surf. Coatings Technol.*, vol. 202, no. 17, pp. 4114–4120, 2008.
[75] J. H. Lehman, M. Terrones, E. Mansfield, K. E. Hurst, and V. Meunier, “Evaluating the characteristics of multiwall carbon nanotubes,” *Carbon*, vol. 49, no. 8. pp. 2581–2602, 2011.
[76] J. Gavillet, A. Loiseau, C. Journet, F. Willaime, F. Ducastelle, and J. C. Charlier, “Root-growth mechanism for single-wall carbon nanotubes.,” *Phys. Rev. Lett.*, vol. 87, no. 27 Pt 1, p. 275504, Dec. 2001.
[77] A. Goyal, A. Kumar, P. K. Patra, S. Mahendra, S. Tabatabaei, P. J. J. Alvarez, G. John, and P. M. Ajayan, “In situ synthesis of metal nanoparticle embedded free standing multifunctional PDMS films,” *Macromol. Rapid Commun.*, vol. 30, no. 13, pp. 1116–1122, 2009.
[78] K. A. Wepasnick, B. A. Smith, J. L. Bitter, and D. Howard Fairbrother, “Chemical and structural characterization of carbon nanotube surfaces,” *Analytical and Bioanalytical Chemistry*, vol. 396, no. 3. pp. 1003–1014, 2010.
[79] O. Byl, J. Liu, and J. T. Yates, “Etching of carbon nanotubes by ozone-a surface area study,” *Langmuir*, vol. 21, no. 9, pp. 4200–4204, 2005.
[80] A. Pevzner, Y. Engel, R. Elnathan, T. Ducobni, M. Ben-Ishai, K. Reddy, N. Shpaisman, A. Tsukernik, M. Oksman, and F. Patolsky, “Knocking down highly-ordered large-scale nanowire arrays,” *Nano Lett.*, vol. 10, no. 4, pp. 1202–1208, 2010.
[81] E. Mansfield, A. Kar, and S. A. Hooker, “Applications of TGA in quality control

of SWCNTs," *Anal. Bioanal. Chem.*, vol. 396, no. 3, pp. 1071–1077, 2010.
[82] A. C. Ferrari, J. C. Meyer, V. Scardaci, C. Casiraghi, M. Lazzeri, F. Mauri, S. Piscanec, D. Jiang, K. S. Novoselov, S. Roth, and A. K. Geim, "Raman spectrum of graphene and graphene layers," *Phys. Rev. Lett.*, vol. 97, no. 18, 2006.
[83] A. C. Ferrari, "Raman spectroscopy of graphene and graphite: Disorder, electron-phonon coupling, doping and nonadiabatic effects," *Solid State Commun.*, vol. 143, no. 1–2, pp. 47–57, 2007.
[84] M. S. Dresselhaus, G. Dresselhaus, R. Saito, and A. Jorio, "Raman spectroscopy of carbon nanotubes," *Phys. Rep.*, vol. 409, no. 2, p. 47, 2005.
[85] M. S. Dresselhaus, A. Jorio, M. Hofmann, G. Dresselhaus, and R. Saito, "Perspectives on carbon nanotubes and graphene Raman spectroscopy," *Nano Letters*, vol. 10, no. 3. pp. 751–758, 2010.
[86] S. Esconjauregui, M. Fouquet, B. C. Bayer, C. Ducati, R. Smajda, S. Hofmann, and J. Robertson, "Growth of ultrahigh density vertically aligned carbon nanotube forests for interconnects," *ACS Nano*, vol. 4, no. 12, pp. 7431–7436, 2010.
[87] A. H. Barber, S. R. Cohen, and H. Daniel Wagner, "Static and dynamic wetting measurements of single carbon nanotubes," *Phys. Rev. Lett.*, vol. 92, no. 18, pp. 186103–1, 2004.
[88] K. K. S. Lau, J. Bico, K. B. K. Teo, M. Chhowalla, G. A. J. Amaratunga, W. I. Milne, G. H. McKinley, and K. K. Gleason, "Superhydrophobic Carbon Nanotube Forests," *Nano Lett.*, vol. 3, no. 12, pp. 1701–1705, 2003.
[89] C. Journet, S. Moulinet, C. Ybert, S. T. Purcell, and L. Bocquet, "Contact angle measurements on superhydrophobic Carbon Nanotube Forests : effect of fluid pressure," *Europhys. Lett.*, vol. 71, pp. 104–109, 2005.
[90] J. Vincent, "Basic Elasticity and Viscoelasticity," *Struct. Biomater.*, pp. 1–28, 2012.
[91] a Montazeri, K. Pourshamsian, and M. Riazian, "Viscoelastic properties and determination of free volume fraction of multi-walled carbon nanotube/epoxy composite using dynamic mechanical thermal analysis," *Mater. Des.*, vol. 36, pp. 408–414, 2012.
[92] A. Montazeri, K. Pourshamsian, and M. Riazian, "Viscoelastic properties and determination of free volume fraction of multi-walled carbon nanotube/epoxy composite using dynamic mechanical thermal analysis," *Mater. Des.*, vol. 36, pp. 408–414, 2012.
[93] S. J. Fang, W. Chen, T. Yamanaka, and C. R. Helms, "Comparison of Si surface roughness measured by atomic force microscopy and ellipsometry," *Appl. Phys. Lett.*, p. 2837, 1995.